
Multi-scale Graph Autoregressive Modeling: Molecular Property Prediction via Next Token Prediction

Zhuoyang Jiang^{1 2} Yaosen Min² Peiran Jin² Lei Chen¹

Abstract

We present **Connection-Aware Motif Sequencing (CamS)**, a graph-to-sequence representation that enables decoder-only Transformers to learn molecular graphs via standard next-token prediction (NTP). For molecular property prediction, SMILES-based NTP scales well but lacks explicit topology, whereas graph-native masked modeling captures connectivity but risks disrupting the pivotal chemical details (e.g., activity cliffs). CamS bridges this gap by serializing molecular graphs into structure-rich causal sequences. CamS first mines data-driven connection-aware motifs. It then serializes motifs via scaffold-rooted breadth-first search (BFS) to establish a stable core-to-periphery order. Crucially, CamS enables hierarchical modeling by concatenating sequences from fine to coarse motif scales, allowing the model to condition global scaffolds on dense, uncorrupted local structural evidence. We instantiate **CamS-LLaMA** by pre-training a vanilla LLaMA backbone on CamS sequences. It achieves state-of-the-art performance on MoleculeNet and the activity-cliff benchmark MoleculeACE, outperforming both SMILES-based language models and strong graph baselines. Interpretability analysis confirms that our multi-scale causal serialization effectively drives attention toward cliff-determining differences.

1. Introduction

Molecular property prediction is a core challenge in drug discovery (Wu et al., 2018) and has increasingly become a primary benchmark for “Foundation Models (FM) for Science.” (Khan et al., 2025) Within FM paradigm, the training recipe has standardized: **decoder-only Transform-**

ers trained via next-token prediction (NTP) serve as the dominant engine for scale and generalization (Wang et al., 2024; Xia et al., 2025; Zhang et al., 2025). Consequently, as the core components of these training stacks become heavily optimized, the pragmatic research focus shifts away from bespoke backbone re-design toward optimizing the **input representation** to fit this proven architecture (Touvron et al., 2023). However, a critical gap remains: current NTP-based molecular models, which largely rely on 1D SMILES strings, fail to explicitly capture graph topology and consequently trail behind specialist graph models in predictive accuracy (Xia et al., 2025).

Conversely, graph-native methods explicitly model topology but typically **depart from pure decoder-only NTP**, instead adopting hybrid architectures or objectives that involve, to varying degrees, **input corruption** (e.g., masked node prediction) (Li et al., 2023; Shehzad et al., 2024; Lu et al., 2025; Kong et al., 2025). While sophisticated strategies—such as incorporating global knowledge nodes or avoiding random masking—have been developed to **mitigate** the information loss caused by masking (Li et al., 2023; Rong et al., 2020; Liu et al., 2024; You et al., 2020; Xu et al., 2021), these methods remain fundamentally bound by the corruption-coverage trade-off (Wettig et al., 2023). This limitation is particularly acute in *activity-cliff* scenarios, where a single atomic change triggers a drastic property shift; masking the local neighborhood of a critical functional group effectively removes the precise evidence needed to discern such subtle differences. Standard NTP, by contrast, offers a dense supervision signal without corrupting the visible prefix context (Clark et al., 2020), yet it lacks a **representation interface** that exposes graph connectivity as effectively as text.

To bridge this gap, we propose **Connection-Aware Motif Sequencing (CamS)**, a tokenizer-level interface that makes molecular graphs directly learnable by standard decoder-only NTP through a three-stage design. First, to ensure information efficiency while preserving semantics, we adapt byte-pair encoding (BPE)-style mining on molecular graphs (Shibata et al., 1999; Geng et al., 2023; Shen & Poczos). This produces motif vocabulary with frequent merge operation and introduces a tunable molecular scale that allows direct granularity control. To ensure faithful encoding of

¹The Hong Kong University of Science and Technology (Guangzhou), Guangzhou, China ²Zhongguancun academy, Beijing, China. Correspondence to: Yaosen Min <yaosenmin@zgc.ac.cn>, Peiran Jin <jinpeiran@bjzgc.edu.cn>.

fine-grained chemical detail, we further integrate a Single-Atom Vocabulary Closure (SAVC) mechanism. Second, to make the graph autoregressive-ready, we partition the molecule into a BPEGraph at a specific scale and serialize it via scaffold-rooted breadth-first search (BFS) (Bundy & Wallen, 1984). This produces a CamS subsequence with a stable **Intra-scale Order**, moving from the global core to peripheral functional groups. Third, and most critically, to construct a hierarchical context, we concatenate subsequences from fine to coarse. This strategy circumvents the trade-off between scales and establishes an **Inter-scale Order** in the final CamS sequence, enabling high-level motifs to be predicted by conditioning on dense, uncorrupted fine-scale evidence. Collectively, these steps unify substructure compression and serialization through a **dual-causal ordering**—sequencing motifs within each scale and stacking scales hierarchically—to enable the model to comprehend global scaffolds based on explicit, uncorrupted local structural evidence.

Built on CamS, we instantiate **CamS-LLaMA** by pre-training a native decoder-only backbone with standard NTP on CamS sequences, keeping the architecture and objective unchanged (Touvron et al., 2023). To keep attribution controlled, we inject only a lightweight molecular fingerprint (Cereto-Massagué et al., 2015) prior during downstream fine-tuning, while keeping pre-training purely sequence/structure-driven. Across MoleculeNet (Wu et al., 2018) and the activity-cliff stress test MoleculeACE (Van Tilborg et al., 2022), CamS-LLaMA achieves state-of-the-art performance at a comparable model scale to strong graph self-supervised learning baselines, despite relying on substantially weaker priors (Li et al., 2023). Beyond accuracy, we provide mechanism-level evidence. Targeted **ablation studies** confirm that multi-scale concatenation is the key driver of performance, while **interpretability** analysis reveals that the causal serialization effectively drives attention toward cliff-determining structural differences.

Contributions. (1) **Methodological Framework:** We introduce CamS, a unified graph-to-causal-sequence interface that resolves the conflict between graph topology preservation and scalable autoregressive training, enabling NTP to function as a structure-native objective. (2) **Empirical Validation:** We demonstrate that CamS-LLaMA achieves state-of-the-art performance on MoleculeNet and MoleculeACE benchmarks. Mechanism analysis reveals that the multi-scale causal context explicitly improves attention focus on subtle, activity-determining structural edits. (3) **Implementation Recipe:** We provide a reproducible pipeline—from the CamS-tokenizer to the CamS-LLaMA—establishing a robust baseline for applying standard foundation model architectures to molecular science.

2. Related Work

2.1. Molecular Property Prediction within Foundation Models Paradigm

Molecular property prediction is increasingly adopting a foundation model approach: large-scale Transformer pre-training followed by fine-tuning for diverse property endpoints (Awais et al., 2025; Xia et al., 2025). One approach adopts standard large language model (LLM) methodology by representing molecules as SMILES strings and pre-training decoder-only models via NTP (Xia et al., 2025; Cai et al., 2025). This leverages mature LLM infrastructure and enables straightforward large-scale training. However, SMILES is not structure-native, weakening topology-based signals. String-based edits often misalign with actual chemical changes, and performance consistently trails strong graph-native methods on property prediction tasks (Xia et al., 2025). Alternatively, graph-native foundation models directly process molecular graphs to preserve connectivity and local topology (You et al., 2021; Liu et al.; You et al., 2020; Xu et al., 2021). High-performing methods typically employ encoder-only Graph Transformers (Shehzad et al., 2024) designed for property prediction. While effective, these models deviate from the vanilla decoder-only NTP approach that exhibits superior generalization and scalability (Li et al., 2023; Rong et al., 2020). More recent structural foundation models integrate graphs with autoregressive components but frequently depend on additional objectives (often incorporating 3D structure) and learned molecular encoders rather than pure tokenizer-level NTP (Kong et al., 2025; Lu et al., 2025; Zhang et al., 2025).

2.2. Molecular Tokenization Strategies

Within a foundation model paradigm, tokenizer design becomes a key interface for scaling LLMs. In NLP, BPE yields strong compression via simple frequency-based merges without training an extra tokenizer model. Molecular tokenization spans string-based and graph-based methods (Wang et al., 2019; Liu et al., 2023). String-based schemes operate on SMILES (Weininger, 1988) or related linearizations (Krenn et al., 2022), while graph-based schemes have evolved from basic node/edge-level units to fragment-level motifs (Liu et al., 2023). Some rule-based motif tokenizations rely on limited handcrafted chemistry rules (Zhang et al., 2021); triplet tokenizations, as used in KPGT (Knowledge-guided Pre-training of Graph Transformer), show that enriching a node token with only one extra atom can substantially boost property prediction (Li et al., 2023); ring-or-path-based (Wollschläger et al., 2024) and tree-based (Jin et al., 2018) schemes also expose substructures at different granularities; some other works learn tokenization via trainable rules (Sun et al., 2024) or by training a GNN as a tokenizer (Liu et al., 2023; Luo et al.). Particularly

noteworthy are data-driven motif mining approaches that adapt BPE idea to graphs to obtain reusable, multi-scale fragments with strong compression and minimal reliance on manually designed rules or additional trained models (Geng et al., 2023; Shen & Poczos; Kong et al., 2022). In addition, cross-level tokenization schemes, which combine motifs at different structural levels, also provide complementary design ideas (Ji et al., 2022; Chen et al.).

3. Method

Our molecular representation must satisfy two requirements: (1) chemical fidelity, i.e., sensitivity to pharmacophore-level structures and their topology; and (2) autoregressive foundation model compatibility, i.e., a compressed interface naturally aligned with an NTP paradigm (Touvron et al., 2023). Motivated by this, we propose **Connection-Aware Motif Sequencing (CamS)**, which segments molecular graphs into reusable frequent motifs and, crucially, serializes the motif graph into multi-scale connection-aware causal sequences compatible with NTP pre-training (Section 3.1). Built on CamS, **CamS-LLaMA** performs large-scale autoregressive pre-training and injects a only lightweight fingerprint prior during downstream fine-tuning (Section 3.2). Finally, we analyze the characteristics and advantages of multi-scale CamS autoregressive modeling by comparing it with Graphformer-style modeling (Section 3.3).

3.1. CamS-Tokenizer

The CamS-tokenizer framework operates in three logical phases to bridge graph topology and scalable NTP. (1) **CamS Vocabulary Construction**: we maintain a robust vocabulary via **BPE-style mining** and **Single-Atom Vocabulary Closure (SAVC)** (Section 3.1.1). (2) **Per-Scale Encoding**: molecules are partitioned into motif graphs (BPE-Graph) and serialized into single-scale *CamS subsequences* via scaffold-anchored BFS (Section 3.1.2). (3) **Cross-Scale Concatenation**: subsequences are organized in a fine-to-coarse order to form the final *CamS sequence*, enabling multiscale autoregressive modeling (Section 3.1.3). Full details are in Appendix A.

3.1.1. SUBSTRUCTURE LEVEL: CAMS VOCABULARY

BPE-style Mining. Following (Geng et al., 2023; Shen & Poczos), we first learn an ordered list of merge operations \mathcal{O} from co-occurrence statistics. We then apply \mathcal{O} to the corpus to mine the resulting subgraphs. This yields the **BPEMotif** set (frequent subgraphs with connectivity patterns) and the base **BPE-SAV** (Single-Atom Vocabulary with connectivity patterns) naturally captured during mining.

Single-Atom Vocabulary Closure (SAVC). While generation operates within a closed vocabulary, predictive encod-

ing encounters unseen atom states. Standard GraphBPE tokenizers greedily match largest motifs and recursively back off; if a specific atom-connectivity form is absent, it collapses to [UNK]. This erases chemical details (e.g., element type) and creates Causal Information Breakpoints in the autoregressive stream. To prevent this, SAVC constructs the *BPE-SAV Back-off* via two strategies: (1) enumerating connection-aware tokens for all typical valences, and (2) mapping rare atypical forms of element X to $\langle X_AltForm \rangle$ rather than $\langle UNK \rangle$.

The final **CamS Vocabulary** Σ is the union of BPEMotif, the complete SAV (BPE-SAV \cup Back-off), and special tokens mapped to unique integers. This guarantees that every atom is covered by either a high-level motif or a precise single-atom descriptor (details in Appendix A.1).

3.1.2. PER-SCALE ENCODING

Given a vocabulary scale s (determined by the iteration count of merge operations), encoding a molecule M involves three stages to generate a single-scale **CamS subsequence**.

BPEGraph Construction. We apply the prefix of merge operations to M , inducing a partition of atoms into non-overlapping fragments. This forms the BPEGraph $G_s = (V_s, E_s)$, where nodes $V_s \subset \Sigma$ are connection-aware motifs/atoms and E_s represents chemical bonds between them.

Serialization (Intra-scale Order). To adapt the graph for decoder-only NTP, we serialize V_s into an ordered list via Breadth-First Search (BFS). We select the motif with the largest atom count (typically the core scaffold) as the root. This strategy prioritizes global backbone structure before local substitutions (Zhang et al., 2021), establishing a stable **Center-to-Periphery** causal order.

ID Extraction. Mapping the ordered nodes to their indices in Σ yields the single-scale **CamS subsequence** $X^{(s)} = (x_1^{(s)}, \dots, x_{L_s}^{(s)})$.

3.1.3. CROSS-SCALE CONCATENATION

Single-scale tokenization faces a trade-off: coarse scales capture global scaffolds but offer low resolution, while fine scales preserve atomic details but fragment high-level structures (e.g., pharmacophores). CamS resolves this by constructing a multi-scale causal context. We tokenize the molecule at multiple scales (e.g., $s \in \{1K, 7K, 27K, 67K\}$) by slicing \mathcal{O} . The resulting subsequences are concatenated in a fixed **Fine-to-Coarse** order (Inter-scale Order) to form the final **CamS sequence X**:

$$\mathbf{X} = [[\text{BOS}], X^{(1K)}, [\text{CONCAT}], X^{(7K)}, [\text{CONCAT}], X^{(27K)}, [\text{CONCAT}], X^{(67K)}, [\text{EOS}]]. \quad (1)$$

During training, this **CamS token stream** allows the model to leverage high-resolution local topology (fine scales) as a prefix to condition the prediction of global scaffolds (coarse scales). This effectively embeds bottom-up structural composition into the autoregressive objective without architectural modifications (analysis in Section 3.3).

3.2. CamS-LLaMA

CamS-LLaMA follows a representation-model co-design principle. Section 3.1 maps a molecular graph $G = (V, E)$ into a multi-scale, connection-aware causal sequence $X = (x_1, \dots, x_T)$ (Eq. (1)) under vocabularies $\Sigma_{1K} \subset \Sigma_{7K} \subset \Sigma_{27K} \subset \Sigma_{67K} \triangleq \Sigma$, via BFS-ordered motif traversals $\mathcal{T}_s(G)$ and token mapping $x_\ell^{(s)} = \iota_s(\mathcal{T}_\ell^{(s)}) \in \Sigma_{sK} \subseteq \Sigma$. The key point is that this graph-to-causal-sequence interface is intentionally designed to be transparent to a vanilla decoder-only Transformer: it exposes topology through a causal order and a fine-to-coarse hierarchy, so we can train with standard NTP without modifying the LLaMA backbone. Based on this interface, CamS-LLaMA follows the foundation model protocol: (1) self-supervised autoregressive pre-training on CamS sequences (figure 1 bottom right), and (2) supervised fine-tuning with a minimal structural prior (fingerprints) injected only at fine-tuning time (figure 1 bottom left).

3.2.1. AUTOREGRESSIVE PRE-TRAINING VIA NTP

CamS-LLaMA adopts a standard LLaMA-style decoder (Touvron et al., 2023); in pre-training, every CamS token list is treated as an ordinary token sequence in the shared vocabulary Σ and is consumed by the backbone under the usual causal mask, with no graph-specific architectural modification. Concretely, each molecule yields five CamS sequence views $\{X_1, X_7, X_{27}, X_{67}, X\}$: four single-scale BFS sequences tokenized with $\Sigma_{1K}/\Sigma_{7K}/\Sigma_{27K}/\Sigma_{67K}$, plus the concatenated multi-scale sequence X in Eq. (1); we treat each view as one NTP training instance (details in Appendix A.3). Given any view $X = (x_1, \dots, x_T)$, token embeddings form $\mathbf{H}^{(0)}$, which is transformed by L causal self-attention blocks into $\mathbf{H}^{(L)}$; a tied output projection then yields $p_\theta(x_{t+1} \mid x_{\leq t})$.

Importantly, CamS changes what the model can condition on under the same NTP objective by reshaping the prefix context through fine-to-coarse concatenation (Eq. (1)). Let $\mathcal{I}_{\text{tok}} \subseteq \{1, \dots, T-1\}$ be valid prediction positions in X (excluding [BOS], [CONCAT], [EOS]), and x_{t+1}^* be the ground-truth next token. The NTP loss is

$$\mathcal{L}_{\text{NTP}}(\theta; X) = - \sum_{t \in \mathcal{I}_{\text{tok}}} \log p_\theta(x_{t+1}^* \mid x_{\leq t}). \quad (2)$$

Because X concatenates BFS sequences from fine to coarse scales (Eq. (1)), the conditioning prefix $x_{\leq t}$ has an explicit hierarchy: for t in X_{67} (highest-merge segment), the model

conditions on all finer-scale tokens (X_1, X_7, X_{27}) plus the coarse prefix. Thus, coarse-scale prediction errors propagate through attention to both coarse predecessors and the entire fine-scale prefix, providing a **fine-to-coarse causal credit assignment** under a fully standard decoder.

On the pre-training corpus \mathcal{D}_{pre} , we minimize

$$\min_{\theta} \mathbb{E}_{X \sim \mathcal{D}_{\text{pre}}} [\mathcal{L}_{\text{NTP}}(\theta; X)], \quad (3)$$

learning general-purpose molecular representations purely from CamS sequences, without any downstream labels or extra descriptors.

3.2.2. FINE-TUNING WITH FINGERPRINT INJECTION

Many molecular pre-training methods inject rich hand-crafted descriptors early (e.g., during pre-training) (Li et al., 2023). In contrast, we keep CamS as the primary representation and inject only one widely-used structural prior—a fingerprint—only during fine-tuning, to make the contribution of CamS representations more attributable and controlled.

We treat the fingerprint as a virtual global token. For each molecule, a fingerprint vector

$$\mathbf{f} \in \mathbb{R}^{D_{\text{fp}}}, \quad (4)$$

is projected to the model hidden size:

$$\mathbf{f}' = W_{\text{fp}} \mathbf{f}, \quad W_{\text{fp}} \in \mathbb{R}^{H \times D_{\text{fp}}}, \quad (5)$$

and prepended to token embeddings:

$$\mathbf{H}_{\text{ft}}^{(0)} = [\mathbf{f}'; \mathbf{e}_1; \dots; \mathbf{e}_T] \in \mathbb{R}^{(T+1) \times H}. \quad (6)$$

With a modified causal mask, all positions can attend to this global token. After L layers:

$$\mathbf{H}_{\text{ft}}^{(L)} = [\mathbf{h}_0^{(L)}; \mathbf{h}_1^{(L)}; \dots; \mathbf{h}_T^{(L)}]. \quad (7)$$

We use the global token representation $\mathbf{u}^{(i)} = \mathbf{h}_0^{(L)}$ for prediction (a decoder-only analogue of [CLS]).

For classification:

$$\hat{\mathbf{y}}^{(i)} = \text{softmax}(W_2 \sigma(W_1 \mathbf{u}^{(i)})),$$

$$\mathcal{L}_{\text{cls}}(\theta, \phi) = -\frac{1}{B} \sum_{i=1}^B \log \hat{\mathbf{y}}_{y^{(i)}}^{(i)}. \quad (8)$$

For regression:

$$\hat{y}^{(i)} = W_2 \sigma(W_1 \mathbf{u}^{(i)}),$$

$$\mathcal{L}_{\text{reg}}(\theta, \phi) = \frac{1}{B} \sum_{i=1}^B (\hat{y}^{(i)} - y^{(i)})^2. \quad (9)$$

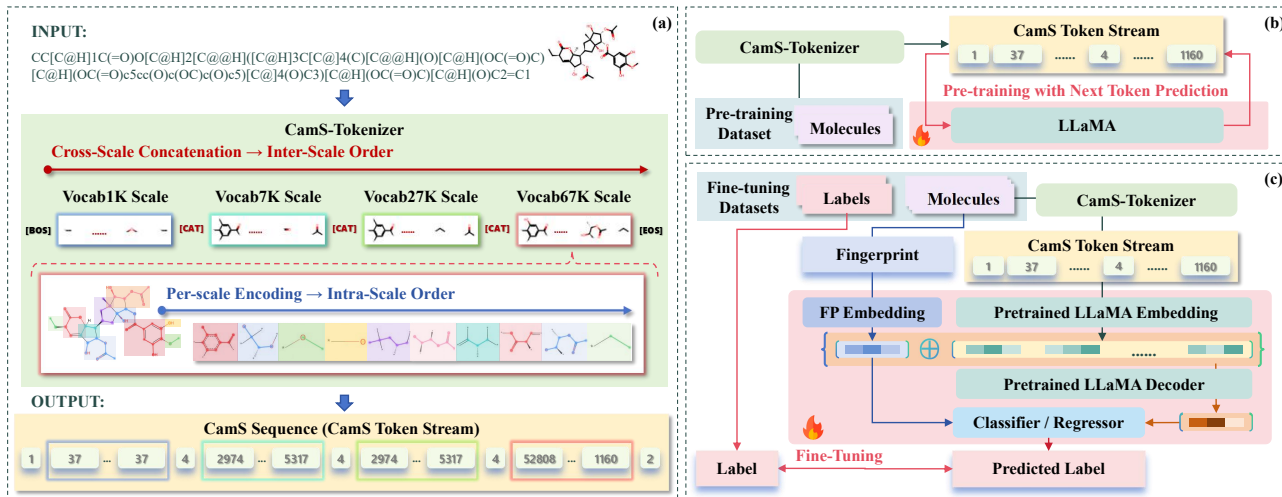


Figure 1. The overall framework of CamS-LLaMA. (a) **CamS-Tokenizer**: Molecules are transformed into multi-scale causal sequences. Through **Per-scale Encoding**, motif graphs are serialized via Scaffold-rooted BFS (Intra-Scale Order) to establish CamS Subsequence, followed by **Cross-Scale Concatenation** to arrange subsequences into a final CamS Sequence from fine to coarse granularities (Inter-Scale Order). (b) **Pre-training Pipeline**: The model is pre-trained on CamS Token Lists using a standard LLaMA via NTP, learning to aggregate structural information. (c) **Fine-tuning Pipeline**: During downstream tasks, the pre-trained weights are transferred, and a lightweight fingerprint prior is injected (via projection, prepending in embedding layer and fusion in classifier or regressor) to take part in the prediction of specific properties.

Fine-tuning minimizes

$$\min_{\theta, \phi} \mathbb{E}_{(X, \mathbf{f}, y) \sim \mathcal{D}_{\text{task}}} [\mathcal{L}_{\text{cls/reg}}(\theta, \phi; X, \mathbf{f}, y)]. \quad (10)$$

This keeps pre-training purely sequence/structure-driven, while using fingerprints as a lightweight and controlled prior only when optimizing for downstream targets.

3.3. CamS Representation vs. Graph Transformer

We analyze CamS-LLaMA and graph transformer-style models (e.g., KPGT) within a unified framework of **Token-Level Graph-Structured Deep Feature Construction**. We show that CamS yields (1) a denser and multi-view direct supervision signal and (2) a hierarchical inductive bias that are mathematically distinct from standard masked-node prediction (MNP). Detailed derivations and supporting discussions are provided in Appendix B.

3.3.1. UNIFIED FRAMEWORK.

Let $G = (V, E)$ be a molecular graph. Both paradigms construct a token graph $\mathcal{G}_{\text{tok}} = (\mathcal{V}_{\text{tok}}, \mathcal{E}_{\text{tok}})$ and perform L layers of propagation:

$$\begin{aligned} \mathbf{H}^{(l+1)} &= \text{Agg}(\mathbf{A}^{(l)} \text{Val}(\mathbf{H}^{(l)})), \\ \mathbf{A}_{ij}^{(l)} &\propto \exp\left(\frac{\mathbf{q}_i^\top \mathbf{k}_j}{\sqrt{d}} + \psi_{ij}\right). \end{aligned} \quad (11)$$

where $\mathbf{H}^{(l)}$ are token embeddings, $\mathbf{q}_i, \mathbf{k}_j$ are projections of $\mathbf{H}^{(l)}$, and ψ_{ij} encodes the structural bias or causal mask.

Graphformer (Flat/Static Bias). \mathcal{V}_{tok} corresponds to single-scale atoms or triplets. ψ_{ij} encodes **static** structural biases (e.g., shortest-path-distance bias injected into attention) independent of token content, yielding an isotropic receptive field at a given graph distance (Ying et al., 2021).

CamS-LLaMA (Hierarchical/Causal Flow). \mathcal{V}_{tok} comprises multi-scale motifs $\{v^{(s)}\}$, where the same molecule is re-represented across scales. ψ_{ij} is determined by the causal mask $\mathcal{M}_{\text{causal}}$, enforcing a directed flow where coarse-scale tokens attend to fine-scale predecessors. This turns cross-scale aggregation into a learned, anisotropic connectivity along the sequence.

3.3.2. INFORMATION-THEORETIC CONTEXT ANALYSIS.

We contrast NTP with MNP. Let x_t be a target token and let Z_t denote its uncorrupted evidence set (e.g., the causal history for CamS coarse-scale tokens). MNP observes a stochastically corrupted context $\tilde{Z}_t = \mathcal{M}(Z_t)$ via random masking.

Proposition 3.1 (Context Information Inequality). *For any non-trivial masking channel \mathcal{M} , we have*

$$I(x_t; Z_t) \geq I(x_t; \tilde{Z}_t). \quad (12)$$

Sketch. The inequality follows from the Data Processing

Inequality (DPI): masking is a stochastic post-processing of Z_t that cannot increase mutual information (Cover, 1999). In graph MNP, this loss of information is exacerbated by evidence-pattern uncertainty: the most relevant local-neighborhood evidence for a masked token may be co-masked, making the conditional distribution unstable across masking patterns. Recent graph pretraining works explicitly mitigate this by masking structured units (e.g., triplets / local subgraphs) or designing structure-guided masking, and by injecting global knowledge tokens (Li et al., 2023; Rong et al., 2020; Liu et al., 2024). In contrast, CamS NTP for coarse-scale tokens conditions on an uncorrupted fine-to-coarse history, avoiding such stochastic evidence loss. This perspective is consistent with classic critiques of Masked Language Modelling (MLM): due to input corruption and factorized prediction over masked positions, it introduces a pre-train–fine-tune discrepancy and neglects dependencies among masked targets (Yang et al., 2019).

3.3.3. GRADIENT FLOW DENSITY.

We define the **Direct Supervision Density** (SD) as the expected fraction of tokens serving as regression targets per update. For a multi-scale sequence with total length $T_{\text{all}} = \sum_{s=1}^S T_s$ and mask ratio ρ :

$$\text{SD}_{\text{NTP}} \approx 1 \gg \text{SD}_{\text{MNP}} = \rho. \quad (13)$$

This trade-off (more predicted tokens vs. more corruption) is central to masked modeling (Wettig et al., 2023). Empirically, KPGT finds the best masking ratio can be as high as $\rho = 0.5$ when using triplet-style tokens and global knowledge nodes to stabilize context (Li et al., 2023). Meanwhile, dense token-level learning signals are known to substantially improve sample efficiency compared to sparse masked-only supervision (Clark et al., 2020). CamS further strengthens this effect by providing multi-view supervision: the same molecule contributes token-level targets repeatedly across scales.

3.3.4. HIERARCHICAL INDUCTIVE BIAS.

Graphformers rely on implicit depth and static structural biases to propagate information. In contrast, CamS injects an explicit structural hierarchy via the multi-scale sequence $X = [X_1, \dots, X_{T_{\text{all}}}]$, and the causal mask ensures coarse-scale predictions have deterministic access to fine-scale details. We hypothesize this is particularly beneficial for activity-cliff regimes, where small local motif edits trigger global property shifts, as it biases the model toward bottom-up composition rules.

4. Experiment

4.1. Experimental Setup

We decouple the pipeline into three stages, using the ChEMBL-34 Dataset for tokenizer training, the Enamine675M Dataset for NTP pre-training, and the MoleculeNet/MoleculeACE Benchmark for downstream fine-tuning and evaluation.

CamS-Tokenizer Training. CamS-tokenizer training is expensive because replaying \mathcal{O} to materialize \mathcal{V} repeatedly invokes RDKit’s subgraph-isomorphism matching (the dominant bottleneck) (Landrum et al., 2021; Ehrlich & Rarey, 2011) to extract motifs and attachment patterns, which is difficult to accelerate. We therefore train the tokenizer once on ChEMBL-34 (Gaulton et al., 2017), a moderately sized yet chemically diverse corpus, at the largest scale (67K). Concretely, we mine an ordered merge list $\mathcal{O} = (o_1, \dots, o_K)$ with $K=685$ merges, apply it to obtain \mathcal{V} , and then perform SAVC to ensure single-atom coverage for common elements. Smaller scales are obtained without retraining by prefix slicing: each scale uses a prefix $\mathcal{O}_{\leq k}$ together with its induced vocabulary subset (i.e., motifs mined by applying $\mathcal{O}_{\leq k}$), where 1K uses $k=0$, 7K/27K use $k=62/210$, and 67K uses $k=685$. Implementation details and full procedures are provided in Appendix A.1.

Pre-training Dataset and Configuration. We instantiate a 16-layer LLaMA-style decoder (hidden size 720, 8 attention heads) using HuggingFace Transformers. For self-supervised pre-training, we use Enamine675M (675M molecules) (Shivanyuk et al., 2007) and optimize NTP (Section 3.2.1). For each molecule, we construct five CamS training sequences: four single-scale BFS sequences tokenized with 1K/7K/27K/67K vocabularies, plus the concatenated multi-scale sequence in Eq. (1). We treat each sequence as one training instance and uniformly shuffle all instances, resulting in roughly $5\times$ as many sequences as molecules. All optimization details (schedule, batch size, steps) are summarized in Appendix C.1.

Downstream Benchmarks and Baselines. We evaluate on MoleculeNet (11 tasks; broad endpoints that probe general-purpose molecular property prediction) (Wu et al., 2018) and MoleculeACE (30 activity-cliff tasks; stress-testing fine-grained structural sensitivity under subtle edits that induce large activity shifts) (Van Tilborg et al., 2022). To enable an apples-to-apples comparison against a recent strong pre-training baseline, we adopt the data splits and evaluation protocol used in KPGT (Li et al., 2023). On MoleculeNet, following KPGT’s setup, we compare primarily against self-supervised pre-training baselines to isolate the effect of (1) representation/tokenization and (2) the pre-training objective. On MoleculeACE, we report the benchmark’s comprehensive ML/DL baselines, since activity cliffs empha-

size discriminating small structural changes where strong feature-based methods remain competitive. Unless stated otherwise, CamS-LLaMA is kept at $\sim 100\text{M}$ parameters (comparable to KPGT); fingerprints are injected only during fine-tuning as a minimal prior, while pre-training is purely sequence-based.

4.2. Main Results

We summarize the main comparisons in Table 1 (MoleculeNet) and Table 2 (MoleculeACE).

General property prediction (MoleculeNet). Table 1 shows that CamS-LLaMA achieves overall state-of-the-art on MoleculeNet under a comparable model scale to KPGT ($\sim 100\text{M}$): it slightly improves the average AUROC in classification (0.845 vs. 0.843) and the average RMSE in regression (1.172 vs. 1.175). We also win 6/11 individual tasks (5/8 classification and 1/3 regression), and improve over the previous best self-supervised learning baselines by a clear margin (AVG-AUROC: 0.845 vs. 0.825; AVG-RMSE: 1.172 vs. 1.272). Notably, this is achieved with weaker prior injection: unlike KPGT, which explicitly feeds rich handcrafted descriptors, we keep pre-training purely sequence-based and inject only a lightweight fingerprint prior during downstream fine-tuning. Full per-baseline results and extended tables are provided in Appendix D.

Activity Cliff Prediction (MoleculeACE). MoleculeACE is a stress-test benchmark for sensitivity to subtle structural edits. In Table 2, CamS-LLaMA achieves the best average RMSE of 0.624, improving over KPGT (0.633, $\sim 1.4\%$ relative) and the strongest non-pre-trained ML baseline SVM_E (0.675, $\sim 7.6\%$ relative). CamS-LLaMA ranks 1st on 17/30 tasks and stays within the top-2 on 29/30 tasks; moreover, it outperforms all ML baselines on 29/30 tasks, with CHEMBL204_{Ki} being the only minor exception (0.709 vs. 0.705 of SVM_E). Mechanistically, CamS makes cliff-driving edits harder to “hide” in near-identical contexts: (1) BPE-mined motifs elevate a local edit into a motif-level token difference (often with distinct size/attachment patterns), (2) BFS rooting/ordering tends to move such motifs to different sequence positions, and (3) multi-scale concatenation further reduces the chance that an edit remains aligned and inconspicuous across all scales simultaneously. Full per-baseline results and extended tables are provided in Appendix D.

Unified Takeaway. Taken together, Tables 1–2 indicate that CamS’s three-stage design (motif mining with single-atom completion \rightarrow causal serialization \rightarrow fine-to-coarse multi-scale concatenation) yields two complementary benefits: (1) **general-purpose representation strength**, by organizing functional-group semantics, attachment patterns, and topology into an NTP-friendly causal context; and (2) **activity-cliff-oriented discriminability**, by exposing

Table 1. Performance on MoleculeNet. Values represent Mean(_{SD}) calculated over 3 random seeds. AVG: Average score across all tasks within each category. Ranking: **Bold** (1st), Underline (2nd), *Italic* (3rd), Gray (Others). Metric: \uparrow denotes higher is better; \downarrow denotes lower is better. Column: Previous Best Baselines denotes the best-performing method excluding KPGT. Reference & Abbreviations: MolF: MolFormer (Wu et al., 2023); Ctxt: Contextpred (Hu et al., 2020); GROV: GROVER (Rong et al., 2020); JOAO (You et al., 2020); GEM (Fang et al., 2022)

TASK	PREVIOUS BEST BASELINES		KPGT	CAMs-LLaMA (OURS)
	METHOD	SCORE		
<i>Classification Tasks (AUROC \uparrow)</i>				
BACE	GEM	<u>0.857</u> _(0.016)	0.855 _(0.014)	0.870 _(0.013)
BBBP	GEM	<i>0.895</i> _(0.024)	<u>0.908</u> _(0.012)	0.942 _(0.015)
CLINTOX	GEM	<i>0.905</i> _(0.027)	0.946 _(0.026)	<u>0.935</u> _(0.017)
ESTROGEN	GEM	<i>0.894</i> _(0.048)	<u>0.906</u> _(0.034)	0.917 _(0.050)
METSTAB	GROV	<i>0.876</i> _(0.046)	<u>0.889</u> _(0.057)	0.891 _(0.059)
SIDER	JOAO	<i>0.640</i> _(0.012)	<u>0.649</u> _(0.011)	0.655 _(0.016)
TOXCAST	GEM	<u>0.733</u> _(0.020)	0.745 _(0.003)	<i>0.724</i> _(0.008)
TOX21	CTXT _{SUP}	<u>0.840</u> _(0.028)	0.848 _(0.017)	0.827 _(0.028)
AVG	GEM	<i>0.825</i>	<u>0.843</u>	0.845
<i>Regression Tasks (RMSE \downarrow)</i>				
ESOL	GEM	<u>0.803</u> _(0.051)	<i>0.804</i> _(0.102)	0.761 _(0.046)
FRESOLV	MOLF	<i>2.322</i> _(0.613)	<u>2.121</u> _(1.025)	2.110 _(0.959)
LIPO	GROV	<u>0.625</u> _(0.007)	0.600 _(0.012)	<i>0.645</i> _(0.023)
AVG	MOLF	<i>1.272</i>	<u>1.175</u>	1.172

cliff-driving edits through motif-level abstraction, position-sensitive causal contexts, and redundant multi-scale views. This motivates a targeted interpretability analysis below, where we test whether the model indeed allocates more attention to cliff-differential tokens than to shared scaffolds, and how this preference varies across scale regions.

4.3. Interpretability: Attention on Activity Cliffs

Interpretability setup and metric. To explain the activity-cliff advantage in Table 2, we test whether CamS-LLaMA preferentially attends to cliff-driving structural differences. Following the MoleculeACE protocol, we construct activity-cliff pairs on the test sets and identify differential vs. shared atom-level activity-cliff point; we then map them to tokens within each scale region of the concatenated CamS sequence (Appendix E). Given the final-layer attention distribution, we compute mean attention on differential tokens (MDTA) and shared tokens (MSTA) within a region and report the relative preference $\text{Rel-DTAP}_s = \frac{\text{MDTA}_s - \text{MSTA}_s}{\text{MSTA}_s + \epsilon} \times 100$, evaluated for each scale region and for the full concatenated sequence. We report the full attention metrics (MDTA/MSTA/Rel-DTAP) in Appendix D.

Findings and implications. Table 3 shows three patterns. (1) Overall preference is positive: on the concatenated sequence, Rel-DTAP is consistently > 0 (14.79% w/o fingerprint; 14.23% w/ fingerprint), indicating that

Table 2. Performance on MoleculeACE (RMSE). **AVG**: Average RMSE across all 30 tasks. Ranking: **Bold** (1st), Underline (2nd), *Italic* (3rd). Metric: \downarrow denotes lower is better. Column: Previous Best Baselines denotes the best-performing method excluding KPGT; Type: ML (Machine Learning), DL (Deep Learning). Reference & Abbreviations: GMAE: GraphMAE (Hou et al., 2022); MBRT: MoleBERT (Xia et al., 2023); GROV: GROVER (Rong et al., 2020); SVM/RF/GBM: Support Vector Machine / Random Forest / Gradient Boosting Machine (Van Tilborg et al., 2022). Descriptors: E: ECFP (Rogers & Hahn, 2010); M: MACCS (Durant et al., 2002).

TASK	PREVIOUS BEST BASELINES			KPGT	CAM-S-LLAMA (OURS)
	METHOD	TYPE	SCORE		
<i>Regression Tasks (RMSE \downarrow)</i>					
CHEMBL1862 _{K1}	GROV	DL	0.668	0.633	0.600
CHEMBL1871 _{K1}	SVM _E	ML	0.668	<u>0.605</u>	0.604
CHEMBL2034 _{K1}	GROV	DL	0.680	0.679	0.619
CHEMBL204 _{K1}	SVM _E	ML	<u>0.705</u>	0.666	0.709
CHEMBL2047 _{EC50}	GMAE	DL	<u>0.578</u>	0.588	0.519
CHEMBL214 _{K1}	GROV	DL	0.663	<u>0.652</u>	0.635
CHEMBL2147 _{K1}	SVM _E	ML	0.612	<u>0.587</u>	0.577
CHEMBL218 _{EC50}	RF _M	ML	0.666	0.625	0.632
CHEMBL219 _{K1}	GROV	DL	0.737	0.718	<u>0.729</u>
CHEMBL228 _{K1}	GROV	DL	0.690	0.669	0.669
CHEMBL231 _{K1}	GROV	DL	0.649	0.610	0.630
CHEMBL233 _{K1}	GROV	DL	0.707	0.691	<u>0.692</u>
CHEMBL234 _{K1}	SVM _E	ML	0.637	0.606	<u>0.624</u>
CHEMBL235 _{EC50}	RF _E	ML	0.637	<u>0.624</u>	0.612
CHEMBL236 _{K1}	SVM _E	ML	0.692	0.655	0.669
CHEMBL237 _{EC50}	SVM _E	ML	0.760	<u>0.716</u>	0.684
CHEMBL237 _{K1}	GROV	DL	0.660	0.678	0.659
CHEMBL238 _{K1}	GBM _E	ML	0.611	<u>0.537</u>	0.537
CHEMBL239 _{EC50}	SVM _E	ML	0.681	0.644	<u>0.647</u>
CHEMBL244 _{K1}	GROV	DL	0.710	<u>0.698</u>	0.696
CHEMBL262 _{K1}	SVM _E	ML	0.703	0.627	<u>0.629</u>
CHEMBL264 _{K1}	SVM _E	ML	0.583	<u>0.574</u>	0.562
CHEMBL2835 _{K1}	RF _E	ML	0.410	0.373	<u>0.384</u>
CHEMBL287 _{K1}	GROV	DL	0.732	<u>0.706</u>	0.685
CHEMBL2971 _{K1}	GBM _E	ML	0.606	0.571	<u>0.574</u>
CHEMBL3979 _{EC50}	GBM _E	ML	0.686	0.669	0.639
CHEMBL4005 _{K1}	SVM _E	ML	0.550	<u>0.559</u>	0.543
CHEMBL4203 _{K1}	MBRT	DL	0.820	0.830	0.787
CHEMBL4616 _{EC50}	SVM _E	ML	0.589	<u>0.587</u>	0.538
CHEMBL4792 _{K1}	SVM _E	ML	0.675	0.619	<u>0.651</u>
AVG	SVM _E	ML	0.675	<u>0.633</u>	0.624

the model, on average, prioritizes cliff-driving differences over shared scaffolds. (2) Preference is scale-dependent: coarse regions (27K/67K) exhibit much stronger preference (24.33%/25.87% w/o fingerprint) than the fewest-merge region (1K, 8.08%), suggesting that coarse motifs provide a more salient interface for highlighting differential substructures, while fine scales contribute weaker but complementary local evidence. (3) Fingerprint acts as a stabilizer rather than a uniform booster: although fingerprint slightly reduces the overall preference, it corrects the anomalous 7K behavior (from -0.18% to 2.10%), consistent with fingerprint providing global guidance that resolves ambiguity at mid-scale tokenizations. Together, these results support the cliff-specific advantage of CamS: multi-scale causal serialization does not merely improve accuracy, but also steers attention toward structurally meaningful differences that

Table 3. **Relative Differential-Token Attention Preference (Rel-DTAP)**. Within each scale region of the concatenated multi-scale sequence, we compute per-molecule $\text{Rel-DTAP}_s = \frac{\text{MDTA}_s - \text{MSTA}_s}{\text{MSTA}_s + \epsilon} \times 100\%$, then average over all molecules from activity-cliff pairs (anchor and partner counted separately). Positive values mean higher per-token attention on differential tokens than on shared tokens.

Scale region	Without FP	With FP
1K	8.08%	4.72%
7K	-0.18%	2.10%
27K	24.33%	23.60%
67K	25.87%	24.00%
CONCAT (all scales)	14.79%	14.23%

drive activity cliffs.

4.4. Ablation Study

Ablation setup. To isolate the contribution of each core component, we evaluate three variants against the full model (Table 4): (1) **w/o FP** removes fingerprint injection during fine-tuning; (2) **Vocab-1K Only** and (3) **Vocab-67K Only** remove multi-scale concatenation by restricting both pre-training and fine-tuning to a single scale. For fair comparison, single-scale variants keep the pre-training budget matched to the full model (details in Appendix C.1).

Multi-scale concatenation is indispensable. The full model consistently outperforms both single-scale variants across all benchmarks (e.g., MolNet-CIs 0.845 vs. 0.833/0.818; MolNet-Reg 1.172 vs. 1.215/1.329; MolACE 0.624 vs. 0.641/0.649), confirming that multi-scale concatenation is not a minor engineering choice but the key mechanism that lets coarse-scale reasoning build on fine-scale evidence within one causal context. This directly supports our central claim: multi-scale causal serialization is the representation-level ingredient that makes graph structure learnable by a vanilla decoder-only NTP backbone.

Why 1K-only can beat 67K-only under a fixed NTP budget. Under single-scale training, **Vocab-67K Only** is consistently weaker than **Vocab-1K Only**, especially on regression (1.329 vs. 1.215 RMSE on MolNet-Reg). We interpret this as an over-compression effect: at 67K, sequences for small molecules become very short and each token packs high compositional complexity, which reduces the number of NTP supervision steps per molecule and makes causal dependency learning harder under limited model capacity and training steps. In contrast, 1K produces longer sequences that provide denser autoregressive supervision and more stable causal credit assignment, albeit at the cost of fragmenting scaffold-level semantics. Concat resolves this trade-off by retaining the dense supervision of fine scales while reintroducing scaffold-level abstraction at coarse scales, without

committing to a single “best” vocabulary size.

Fingerprint helps as a stabilizer, with larger gains on activity cliffs. Removing FP causes a modest drop on MoleculeNet (0.845→0.838; 1.172→1.195), but a more pronounced degradation on MoleculeACE (0.624→0.650). This suggests FP acts less as a universal booster and more as a global prior that stabilizes fine-grained decision making when the task demands extreme sensitivity to local edits—consistent with our attention-based analysis, where FP corrects anomalous mid-scale behavior (e.g., the 7K region) rather than uniformly increasing differential-token preference.

Table 4. Ablation study and ranking comparison. Scores represent the average performance across all tasks in the respective benchmarks from Tables 1 and 2. Rank: Global ranking of the specific variant when pooled with the complete set of baseline models. **Previous Best:** The highest-performing baseline excluding KPGT. **Abbreviations:** MolF: MolFormer

METHOD	MOLNET-CLS (↑)		MOLNET-REG (↓)		MOLACE (↓)	
	SCORE	RANK	RMSE	RANK	RMSE	RANK
CAMS-LLAMA (FULL)	0.845	1	1.172	1	0.624	1
– w/o FP	0.838	3	1.195	3	0.650	5
– VOCAB-1K ONLY	0.833	4	1.215	4	0.641	3
– VOCAB-67K ONLY	0.818	6	1.329	7	0.649	4
KPGT	0.843	2	1.175	2	0.633	2
PREVIOUS BEST	0.825 (GEM)	5	1.272 (MOLF)	5	0.675 (SVM _E)	6

5. Conclusion

We introduced **CamS**, a graph-to-sequence interface that enables standard decoder-only Transformers to learn molecular topology via Next Token Prediction. By unifying motif mining, causal serialization, and fine-to-coarse concatenation, CamS constructs a hierarchical context where global scaffolds are conditioned on dense local evidence. The resulting **CAMS-LLaMA** achieves state-of-the-art performance on MoleculeNet and MoleculeACE, surpassing strong graph baselines while relying on minimal priors. Mechanism analysis confirms that this multi-scale causal design is crucial, as it explicitly drives attention toward cliff-determining structural differences. Our work validates that with the right representation interface, generic autoregressive foundation models can serve as powerful, structure-native engines for molecular science.

References

Awais, M., Naseer, M., Khan, S., Anwer, R. M., Cholakkal, H., Shah, M., Yang, M.-H., and Khan, F. S. Foundation models defining a new era in vision: a survey and outlook. *IEEE Transactions on Pattern Analysis and Machine Intelligence*, 2025.

Breiman, L. Bagging predictors. *Machine learning*, 24(2):

123–140, 1996.

- Bundy, A. and Wallen, L. Breadth-first search. In *Catalogue of artificial intelligence tools*, pp. 13–13. Springer, 1984.
- Cai, F., Zacour, K., Zhu, T., Tzeng, T.-R., Duan, Y., Liu, L., Pilla, S., Li, G., and Luo, F. Chemfm as a scaling law guided foundation model pre-trained on informative chemicals. *Communications Chemistry*, 2025.
- Cereto-Massagué, A., Ojeda, M. J., Valls, C., Mulero, M., Garcia-Vallvé, S., and Pujadas, G. Molecular fingerprint similarity search in virtual screening. *Methods*, 71:58–63, 2015.
- Chen, Y., Yao, Q., Zhang, J., Cheng, J., and Bian, Y. Hierarchical graph tokenization for molecule-language alignment. In *Forty-second International Conference on Machine Learning*.
- Chithrananda, S., Grand, G., and Ramsundar, B. Chemberta: large-scale self-supervised pretraining for molecular property prediction. *arXiv preprint arXiv:2010.09885*, 2020.
- Clark, K., Luong, M.-T., Le, Q. V., and Manning, C. D. Electra: Pre-training text encoders as discriminators rather than generators. *arXiv preprint arXiv:2003.10555*, 2020.
- Cover, T. M. *Elements of information theory*. John Wiley & Sons, 1999.
- Cristianini, N. and Scholkopf, B. Support vector machines and kernel methods: the new generation of learning machines. *Ai Magazine*, 23(3):31–31, 2002.
- Durant, J. L., Leland, B. A., Henry, D. R., and Nourse, J. G. Reoptimization of mdl keys for use in drug discovery. *Journal of chemical information and computer sciences*, 42(6):1273–1280, 2002.
- Ehrlich, H.-C. and Rarey, M. Maximum common subgraph isomorphism algorithms and their applications in molecular science: a review. *Wiley Interdisciplinary Reviews: Computational Molecular Science*, 1(1):68–79, 2011.
- Fang, X., Liu, L., Lei, J., He, D., Zhang, S., Zhou, J., Wang, F., Wu, H., and Wang, H. Geometry-enhanced molecular representation learning for property prediction. *Nature Machine Intelligence*, 4(2):127–134, 2022.
- Fix, E. *Discriminatory analysis: nonparametric discrimination, consistency properties*, volume 1. USAF school of Aviation Medicine, 1985.
- Friedman, J. H. Greedy function approximation: a gradient boosting machine. *Annals of statistics*, pp. 1189–1232, 2001.

- Gaulton, A., Hersey, A., Nowotka, M., Bento, A. P., Chambers, J., Mendez, D., Mutowo, P., Atkinson, F., Bellis, L. J., Cibrián-Uhalte, E., et al. The ChEMBL database in 2017. *Nucleic acids research*, 45(D1):D945–D954, 2017.
- Geng, Z., Xie, S., Xia, Y., Wu, L., Qin, T., Wang, J., Zhang, Y., Wu, F., and Liu, T.-Y. De novo molecular generation via connection-aware motif mining. *arXiv preprint arXiv:2302.01129*, 2023.
- Gilmer, J., Schoenholz, S. S., Riley, P. F., Vinyals, O., and Dahl, G. E. Neural message passing for quantum chemistry. In *International conference on machine learning*, pp. 1263–1272. Pmlr, 2017.
- Hamilton, W., Ying, Z., and Leskovec, J. Inductive representation learning on large graphs. *Advances in neural information processing systems*, 30, 2017.
- Hou, Z., Liu, X., Cen, Y., Dong, Y., Yang, H., Wang, C., and Tang, J. GraphMAE: Self-supervised masked graph autoencoders. In *Proceedings of the 28th ACM SIGKDD conference on knowledge discovery and data mining*, pp. 594–604, 2022.
- Hu, W., Liu, B., Gomes, J., Zitnik, M., Liang, P., Pande, V., and Leskovec, J. Strategies for pre-training graph neural networks. In *International Conference on Learning Representations (ICLR)*, 2020.
- Ji, Z., Shi, R., Lu, J., Li, F., and Yang, Y. Relmole: molecular representation learning based on two-level graph similarities. *Journal of Chemical Information and Modeling*, 62(22):5361–5372, 2022.
- Jin, W., Barzilay, R., and Jaakkola, T. Junction tree variational autoencoder for molecular graph generation. In *International conference on machine learning*, pp. 2323–2332. PMLR, 2018.
- Khan, W., Leem, S., See, K. B., Wong, J. K., Zhang, S., and Fang, R. A comprehensive survey of foundation models in medicine. *IEEE Reviews in Biomedical Engineering*, 2025.
- Kimber, T. B., Gagnebin, M., and Volkamer, A. MaxSMI: maximizing molecular property prediction performance with confidence estimation using SMILES augmentation and deep learning. *Artificial Intelligence in the Life Sciences*, 1:100014, 2021.
- Kipf, T. Semi-supervised classification with graph convolutional networks. *arXiv preprint arXiv:1609.02907*, 2016.
- Kong, X., Huang, W., Tan, Z., and Liu, Y. Molecule generation by principal subgraph mining and assembling. *Advances in Neural Information Processing Systems*, 35: 2550–2563, 2022.
- Kong, X., Zhang, Z., Zhang, Z., Jiao, R., Ma, J., Huang, W., Liu, K., and Liu, Y. Unimomo: Unified generative modeling of 3d molecules for de novo binder design. *arXiv preprint arXiv:2503.19300*, 2025.
- Krenn, M., Ai, Q., Barthel, S., Carson, N., Frei, A., Frey, N. C., Friederich, P., Gaudin, T., Gayle, A. A., Jablonka, K. M., et al. Selfies and the future of molecular string representations. *Patterns*, 3(10), 2022.
- Kubinyi, H. *3D QSAR in drug design: volume 1: theory methods and applications*, volume 1. Springer Science & Business Media, 1993.
- Landrum, G., Tosco, P., Kelley, B., Vianello, R., Kawashima, E., Dalke, A., Cole, B., Swain, M., Turk, S., Cosgrove, D., et al. rdkit/rdkit: 2021_09_2 (q3 2021) release. *Zenodo*, 2021.
- Li, H., Zhang, R., Min, Y., Ma, D., Zhao, D., and Zeng, J. A knowledge-guided pre-training framework for improving molecular representation learning. *Nature Communications*, 14(1):7568, 2023.
- Liu, C., Wang, Y., Zhan, Y., Ma, X., Tao, D., Wu, J., and Hu, W. Where to mask: structure-guided masking for graph masked autoencoders. In *International Joint Conference on Artificial Intelligence (33rd: 2024)*, pp. 2180–2188. Association for Computing Machinery (ACM), 2024.
- Liu, S., Wang, H., Liu, W., Lasenby, J., Guo, H., and Tang, J. Pre-training molecular graph representation with 3d geometry. In *International Conference on Learning Representations*.
- Liu, Y., Jin, S., Peng, X., Lu, D., Zeng, L., Sun, Y., Ai, J., Geng, M., and Hu, Y. Pyridazinone derivatives displaying highly potent and selective inhibitory activities against c-met tyrosine kinase. *European Journal of Medicinal Chemistry*, 108:322–333, 2016.
- Liu, Z., Shi, Y., Zhang, A., Zhang, E., Kawaguchi, K., Wang, X., and Chua, T.-S. Rethinking tokenizer and decoder in masked graph modeling for molecules. *Advances in Neural Information Processing Systems*, 36:25854–25875, 2023.
- Lu, S., Lin, H., Yao, L., Gao, Z., Ji, X., Zhang, L., Ke, G., et al. Uni-3dar: Unified 3d generation and understanding via autoregression on compressed spatial tokens. *arXiv preprint arXiv:2503.16278*, 2025.
- Luo, Y., Li, H., Liu, Q., Shi, L., and Wu, X.-M. Node identifiers: Compact, discrete representations for efficient graph learning. In *The Thirteenth International Conference on Learning Representations*.

- Moret, M., Grisoni, F., Katzberger, P., and Schneider, G. Perplexity-based molecule ranking and bias estimation of chemical language models. *Journal of chemical information and modeling*, 62(5):1199–1206, 2022.
- Rogers, D. and Hahn, M. Extended-connectivity fingerprints. *Journal of chemical information and modeling*, 50(5):742–754, 2010.
- Rong, Y., Bian, Y., Xu, T., Xie, W., Wei, Y., Huang, W., and Huang, J. Self-supervised graph transformer on large-scale molecular data. *Advances in neural information processing systems*, 33:12559–12571, 2020.
- Shehzad, A., Xia, F., Abid, S., Peng, C., Yu, S., Zhang, D., and Verspoor, K. Graph transformers: A survey. *arXiv preprint arXiv:2407.09777*, 2024.
- Shen, Y. and Poczós, B. Graphbpe: Molecular graphs meet byte-pair encoding. In *ICML 2024 AI for Science Workshop*.
- Shibata, Y., Kida, T., Fukamachi, S., Takeda, M., Shinohara, A., Shinohara, T., and Arikawa, S. Byte pair encoding: A text compression scheme that accelerates pattern matching. 1999.
- Shivanyuk, A. N., Ryabukhin, S. V., Tolmachev, A., Bogolyubsky, A., Mykytenko, D., Chupryna, A., Heilman, W., and Kostyuk, A. Enamine real database: Making chemical diversity real. *Chemistry today*, 25(6):58–59, 2007.
- Stärk, H., Beaini, D., Corso, G., Tossou, P., Dallago, C., Günnemann, S., and Liò, P. 3d infomax improves gnns for molecular property prediction. In *International Conference on Machine Learning*, pp. 20479–20502. PMLR, 2022.
- Sun, M., Guo, M., Yuan, W., Thost, V., Owens, C. E., Grosz, A. F., Selvan, S., Zhou, K., Mohiuddin, H., Pedretti, B. J., et al. Representing molecules as random walks over interpretable grammars. In *International Conference on Machine Learning*, pp. 46988–47016. PMLR, 2024.
- Touvron, H., Lavril, T., Izacard, G., Martinet, X., Lachaux, M.-A., Lacroix, T., Rozière, B., Goyal, N., Hambro, E., Azhar, F., et al. Llama: Open and efficient foundation language models. *arXiv preprint arXiv:2302.13971*, 2023.
- Van Tilborg, D., Alenicheva, A., and Grisoni, F. Exposing the limitations of molecular machine learning with activity cliffs. *Journal of chemical information and modeling*, 62(23):5938–5951, 2022.
- Veličković, P., Cucurull, G., Casanova, A., Romero, A., Lio, P., and Bengio, Y. Graph attention networks. *arXiv preprint arXiv:1710.10903*, 2017.
- Veličković, P., Fedus, W., Hamilton, W. L., Liò, P., Bengio, Y., and Hjelm, R. D. Deep graph infomax. *arXiv preprint arXiv:1809.10341*, 2018.
- Walters, W. P. and Murcko, M. A. Prediction of ‘drug-likeness’. *Advanced drug delivery reviews*, 54(3):255–271, 2002.
- Wang, S., Guo, Y., Wang, Y., Sun, H., and Huang, J. Smilesbert: large scale unsupervised pre-training for molecular property prediction. In *Proceedings of the 10th ACM international conference on bioinformatics, computational biology and health informatics*, pp. 429–436, 2019.
- Wang, X., Zhang, X., Luo, Z., Sun, Q., Cui, Y., Wang, J., Zhang, F., Wang, Y., Li, Z., Yu, Q., et al. Emu3: Next-token prediction is all you need. *arXiv preprint arXiv:2409.18869*, 2024.
- Weininger, D. Smiles, a chemical language and information system. 1. introduction to methodology and encoding rules. *Journal of chemical information and computer sciences*, 28(1):31–36, 1988.
- Wettig, A., Gao, T., Zhong, Z., and Chen, D. Should you mask 15% in masked language modeling? In *Proceedings of the 17th Conference of the European Chapter of the Association for Computational Linguistics*, pp. 2985–3000, 2023.
- Wollschläger, T., Kemper, N., Hetzel, L., Sommer, J., and Günnemann, S. Expressivity and generalization: Fragment-biases for molecular gnns. In *International Conference on Machine Learning*, pp. 53113–53139. PMLR, 2024.
- Wu, F., Radev, D., and Li, S. Z. Molformer: Motif-based transformer on 3d heterogeneous molecular graphs. In *Proceedings of the AAAI Conference on Artificial Intelligence*, volume 37, pp. 5312–5320, 2023.
- Wu, Z., Ramsundar, B., Feinberg, E. N., Gomes, J., Geniesse, C., Pappu, A. S., Leswing, K., and Pande, V. Moleculenet: a benchmark for molecular machine learning. *Chemical science*, 9(2):513–530, 2018.
- Xia, J., Zhao, C., Hu, B., Gao, Z., Tan, C., Liu, Y., Li, S., and Li, S. Z. Mole-bert: Rethinking pre-training graph neural networks for molecules. 2023.
- Xia, Y., Jin, P., Xie, S., He, L., Cao, C., Luo, R., Liu, G., Wang, Y., Liu, Z., Chen, Y.-J., et al. Nature language model: Deciphering the language of nature for scientific discovery. *arXiv preprint arXiv:2502.07527*, 2025.
- Xiong, Z., Wang, D., Liu, X., Zhong, F., Wan, X., Li, X., Li, Z., Luo, X., Chen, K., Jiang, H., et al. Pushing the boundaries of molecular representation for drug discovery

with the graph attention mechanism. *Journal of medicinal chemistry*, 63(16):8749–8760, 2019.

Xu, M., Wang, H., Ni, B., Guo, H., and Tang, J. Self-supervised graph-level representation learning with local and global structure. In *International conference on machine learning*, pp. 11548–11558. PMLR, 2021.

Yang, Z., Dai, Z., Yang, Y., Carbonell, J., Salakhutdinov, R. R., and Le, Q. V. Xlnet: Generalized autoregressive pretraining for language understanding. *Advances in neural information processing systems*, 32, 2019.

Ying, C., Cai, T., Luo, S., Zheng, S., Ke, G., He, D., Shen, Y., and Liu, T.-Y. Do transformers really perform badly for graph representation? *Advances in neural information processing systems*, 34:28877–28888, 2021.

You, Y., Chen, T., Sui, Y., Chen, T., Wang, Z., and Shen, Y. Graph contrastive learning with augmentations. *Advances in neural information processing systems*, 33:5812–5823, 2020.

You, Y., Chen, T., Shen, Y., and Wang, Z. Graph contrastive learning automated. In *International conference on machine learning*, pp. 12121–12132. PMLR, 2021.

Zeng, X., Xiang, H., Yu, L., Wang, J., Li, K., Nussinov, R., and Cheng, F. Accurate prediction of molecular properties and drug targets using a self-supervised image representation learning framework. *Nature Machine Intelligence*, 4(11):1004–1016, 2022.

Zhang, G., Li, Y., Luo, R., Hu, P., Zhao, Z., Li, L., Liu, G., Wang, Z., Bi, R., Gao, K., et al. Unigenx: Unified generation of sequence and structure with autoregressive diffusion. *arXiv preprint arXiv:2503.06687*, 2025.

Zhang, Z., Liu, Q., Wang, H., Lu, C., and Lee, C.-K. Motif-based graph self-supervised learning for molecular property prediction. *Advances in Neural Information Processing Systems*, 34:15870–15882, 2021.

A. CamS-tokenizer and Graph-to-Sequence Construction

Overview. This section corresponds to the CamS-tokenizer description in Sec. 3.1 (including Secs. 3.1.1, 3.1.2, and 3.1.3) and the multi-view training-instance construction in Sec. 3.2.1. It supplements the main text with implementation-level details of (1) GraphBPE merge learning and Single-Atom Vocabulary Closure (SAVC)(Algs. 1 and Algs. 2), (2) connection-aware motif vocabulary construction and encoding-time unknown recovery (Algs.3 and Algs.4), (3) deterministic scaffold-rooted BFS serialization (Algs. 5), and (4) fine-to-coarse multi-scale concatenation together with NTP loss masking and length handling (Algs. 6)

A.1. Tokenizer Vocabulary Mining and Single-Atom Coverage (GraphBPE + SAVC)

Notation and objects. We start from an RDKit molecule and construct the atom graph $G_0 = (V_0, E_0)$, where each node is an atom and each edge is a chemical bond. A GraphBPE merge list is an ordered sequence of operations $\mathcal{O} = (o_1, \dots, o_K)$, where each operation o_t is a canonical fragment code extracted from the union of two adjacent nodes (details below). Given a prefix $\mathcal{O}_{\leq k}$, applying merges on G_0 yields a motif graph $G = (V, E)$, where each motif node $v \in V$ stores the covered atom set $\text{atom_indices}(v) \subseteq V_0$.

Connection-aware motif representation. Each motif token is stored in a *pair form* $(v_{\text{noConn}}, v_{\text{withConn}})$. The first records the fragment SMILES of the core atoms (no connectors), while the second inserts wildcard connector atoms $*$ at all attachment sites together with explicit bond types, making the token identity *connection-aware*. We materialize these motif pairs by replaying $\mathcal{O}_{\leq k}$ on a tokenizer corpus and inserting connector $*$ atoms for every cut bond (Alg. 3).

Single-atom vocabulary closure (SAVC). A key issue for property prediction is *encoding coverage*: if a rare but meaningful “single-atom + attachment-pattern” form is absent from the mined vocabulary, it would collapse to [UNK] and erase fine-grained distinctions. SAVC addresses this by (1) enumerating common connection-aware single-atom motifs for typical valence states, and (2) adding an element-wise fallback token `X_AltForm` to represent rare/atypical forms. At encoding time, if a queried motif contains exactly one core atom of element X but the exact form is missing, we back off to `X_AltForm` instead of [UNK] (Alg. 2).

Encoding-time unknown recovery. Encoding greedily applies $\mathcal{O}_{\leq k}$ and then maps each resulting motif to its token id. If a motif is still unknown after canonicalization, we recursively split it along its stored merge tree until known motifs are obtained; the recursion stops at single-atom leaves where SAVC backoff applies (Alg. 4).

Algorithm-to-component map. Alg. 1 learns the ordered merge list \mathcal{O} (Sec. 3.1.1). Alg. 3 materializes the connection-aware motif vocabulary by replaying $\mathcal{O}_{\leq k}$ and inserting connector atoms $*$. Alg. 2 specifies SAVC enumeration and `X_AltForm` backoff. Alg. 4 describes encoding-time motif extraction and recursive split for unknown recovery.

A.2. Graph-to-Causal-Sequence Serialization (Traversal and Root Selection)

Motif graph. After applying $\mathcal{O}_{\leq k}$ to G_0 , we obtain a motif graph $G = (V, E)$ where each node $v \in V$ corresponds to a merged fragment with $\text{atom_indices}(v) \subseteq V_0$. An edge $(u, v) \in E$ indicates that at least one original bond in G_0 connects atoms across the two fragments.

Scaffold-rooted BFS order. CamS serializes G into a token sequence by a deterministic scaffold-rooted BFS: we select as root the motif with the largest number of covered atoms (ties broken deterministically, e.g., by smaller node id), and traverse the motif graph breadth-first with a fixed neighbor ordering (e.g., ascending node id). The visitation order defines the final token order, implemented by relabeling motif nodes so that ids $0, 1, \dots$ encode the BFS order (Alg. 5). This yields a stable core-to-periphery causal order aligned with prefix-based NTP (Sec. 3.1.2).

Why no explicit edges in the sequence. We do not append edge/direction tokens: each motif token already includes explicit $*$ attachment sites and bond types, so the attachment *pattern* is part of the token identity (Alg. 3). The BFS order then provides the autoregressive causal structure at the sequence level.

A.3. Multi-scale Concat Construction and Training-Instance Generation

Prefix slicing and scale definition. GraphBPE yields a single merge list $\mathcal{O} = (o_1, \dots, o_K)$. Each vocabulary scale corresponds to a prefix $\mathcal{O}_{\leq k_s}$, which induces a sub-vocabulary $\Sigma_{\leq k_s}$ and a tokenizer ι_s . This “train once, slice many” construction reuses the same learned merge statistics across all scales (Sec. 3.1.3).

Per-molecule views and fine-to-coarse concatenation. For a molecule s , we generate S single-scale views $\{X_{s_1}, \dots, X_{s_S}\}$ by encoding under tokenizers ordered from fine to coarse. We then build one concatenated view by inserting [CONCAT] as separators and keeping only one global [BOS] and [EOS]. Alg. 6 provides the pseudo-code used in implementation (Sec. 3.2.1).

Loss masking and length handling. For NTP training, we exclude [BOS], [EOS], and [CONCAT] positions from prediction targets (typically by setting labels to -100 at these indices). Sequences are padded with [PAD] up to the maximum length; if truncation is needed, we keep boundary tokens [BOS] and [EOS] and truncate the interior span consistently across views.

Algorithm 1 GraphBPE merging-operation learning (ordered merge list \mathcal{O})

```

1: Input: tokenizer corpus  $\mathcal{D}$  (RDKit molecules), max iterations  $K$ , min frequency  $f_{\min}$ 
2: Output: ordered merge list  $\mathcal{O} = (o_1, \dots, o_K)$ 
3: Initialize each molecule  $m \in \mathcal{D}$  with a working graph  $G_m$  where every atom is a node and  $\text{atom\_indices}(i) = \{i\}$ 
4: Compute initial statistics: for each  $m$  and each edge  $(u, v) \in E(G_m)$ , set  $c \leftarrow \text{FragSmiles}(m, \text{atom\_indices}(u) \cup \text{atom\_indices}(v))$  and increment  $\text{stats}[c]$ 
5: for  $t = 1$  to  $K$  do
6:   Select  $o_t \leftarrow \arg \max_c (\text{stats}[c], c)$  (tie-break by lexicographic  $c$  as in code)
7:   if  $\text{stats}[o_t] < f_{\min}$  then
8:     break
9:   end if
10:  Append  $o_t$  to  $\mathcal{O}$ 
11:  Apply  $o_t$  to all molecules that contain it: in each affected  $G_m$ , merge every edge  $(u, v)$  whose union-fragment code equals  $o_t$ 
12:  Update local pair statistics around merged nodes (remove old incident pairs; add new pairs)
13:  Set  $\text{stats}[o_t] \leftarrow 0$  (avoid re-selecting the same operation)
14: end for
    
```

Algorithm 2 Single-Atom Vocabulary Closure (SAVC) with AltForm backoff (implementation-level)

```

1: Input: element set  $\mathcal{E}$ , typical valences  $\text{Val}(X)$ , bond symbols  $\mathcal{B} = \{-, =, \#, :\}$ , wildcard atom  $*$ 
2: Output: basic single-atom token list  $\Sigma_{\text{atom}}$ 
3: for each element  $X \in \mathcal{E}$  do
4:   Add  $X$  (standalone single atom) and  $X_{\text{AltForm}}$  (rare/atypical fallback)
5:   for each  $v \in \text{Val}(X)$  do
6:     for each attachment degree  $d \in \{1, \dots, v\}$  do
7:       for each bond-type tuple  $(b_1, \dots, b_d) \in \mathcal{B}^d$  do
8:         Construct a single-atom fragment SMILES with  $d$  wildcard substituents (use branching if  $d > 1$ ), e.g.
            $*X(*) \dots (*)$  with explicit bonds
9:         Add this motif_with_conn into  $\Sigma_{\text{atom}}$ 
10:      end for
11:    end for
12:  end for
13: end for
14: Encoding-time backoff (MotifVocab.getitem): if a queried motif SMILES is not found after RDKit canonicalization, and it contains exactly one core atom (non-H, non- $*$ ), return the id of X_AltForm; otherwise return [UNK] (code uses id = -1 as unknown sentinel).
    
```

Algorithm 3 Materializing the connection-aware motif vocabulary (motif mining + SAVC integration)

- 1: **Input:** tokenizer corpus \mathcal{D} (SMILES), operation prefix $\mathcal{O}_{\leq k}$, special tokens $\{[\text{PAD}], [\text{BOS}], [\text{EOS}], [\text{UNK}]\}$
- 2: **Output:** motif-pair list $\mathcal{V} = \{(v_{\text{noConn}}, v_{\text{withConn}})\}$ and token set Σ
- 3: **for each** SMILES $s \in \mathcal{D}$ **do**
- 4: Parse s to molecule m ; build $G_0 = (V_0, E_0)$ with atom/bond features
- 5: Apply merges in order $\mathcal{O}_{\leq k}$ on a copy of G_0 to obtain motif graph $G = (V, E)$ where each node v stores $\text{atom_indices}(v) \subseteq V_0$
- 6: Assign each atom $i \in V_0$ to its motif node $\text{bpe_node}(i) \in V$
- 7: **for each** original bond $(i, j) \in E_0$ **do**
- 8: **if** $\text{bpe_node}(i) \neq \text{bpe_node}(j)$ **then**
- 9: Add two connector nodes i^*, j^* with `smarts=*`; attach i^* to i and j^* to j
- 10: Set the bond types of (i, i^*) and (j, j^*) equal to the original bond type of (i, j)
- 11: Include i^* in $\text{atom_indices}(\text{bpe_node}(i))$ and j^* in $\text{atom_indices}(\text{bpe_node}(j))$
- 12: **end if**
- 13: **end for**
- 14: **for each** motif node $v \in V$ **do**
- 15: $v_{\text{noConn}} \leftarrow \text{FragSmiles}(m, \text{atom_indices}(v) \cap V_0)$
- 16: $v_{\text{withConn}} \leftarrow \text{GraphSmiles}(G_0[\text{atom_indices}(v)])$ (contains * connectors)
- 17: Add pair $(v_{\text{noConn}}, v_{\text{withConn}})$ into a frequency counter
- 18: **end for**
- 19: **end for**
- 20: Prepend special tokens; then integrate the SAVC basic vocabulary (Alg. 2) into the pair list

Algorithm 4 GraphBPE encoding with unknown-motif recovery (recursive split)

- 1: **Input:** SMILES s , operations $\mathcal{O}_{\leq k}$, motif vocabulary Σ (lookup by canonical SMILES)
- 2: **Output:** ordered motif list $[(v_{\text{noConn}}, v_{\text{withConn}})]$
- 3: **if** s contains “.” **then**
- 4: Split s into fragments and encode each fragment independently; concatenate motif lists
- 5: **end if**
- 6: Build initial atom graph G_0 and initialize a binary merge tree at each atom node
- 7: Apply $\mathcal{O}_{\leq k}$ in order: for each code o , merge every edge whose union-fragment code equals o (merge also updates the node’s merge tree)
- 8: Relabel nodes to integers and reorder them by scaffold-rooted BFS (Alg. 5)
- 9: Add connector * nodes for every cut bond to build connection-aware subgraphs (Alg. 3)
- 10: Collect motif tokens in BFS order; if a motif is not in Σ , mark it as unknown
- 11: **while** unknown motifs exist **do**
- 12: Pop one unknown motif node and recursively split it into its two children in the stored merge tree
- 13: For each child: if it is in Σ , emit it; else split further; stop at leaves (single-atom motifs), where SAVC backoff applies
- 14: **end while**

Algorithm 5 Scaffold-rooted BFS serialization (root selection + neighbor order)

- 1: **Input:** motif graph $G = (V, E)$ with node attribute $\text{atom_indices}(v)$
- 2: **Output:** a deterministic BFS ordering π (used to relabel nodes)
- 3: Select root $r \leftarrow \arg \max_{v \in V} (|\text{atom_indices}(v)|, -\text{id}(v))$ (tie-break: smaller id)
- 4: Initialize queue with r , mark r visited
- 5: **while** queue not empty **do**
- 6: Pop front node u , append u to ordering π
- 7: Let $\mathcal{N}(u)$ be neighbors of u not yet visited, sorted by ascending node id
- 8: Push neighbors in $\mathcal{N}(u)$ into the queue and mark them visited
- 9: **end while**
- 10: Relabel nodes by π so that the first visited node becomes id 0, the second becomes id 1, etc.

Algorithm 6 Multi-scale CamS concatenation and training-view generation

```

1: Input: SMILES  $s$ , tokenizers  $\{l_{s_1}, \dots, l_{s_S}\}$  ordered fine $\rightarrow$ coarse, special ids bos_id, eos_id, concat_id
2: Output: single-scale views  $\{X_{s_j}\}_{j=1}^S$  and concatenated view  $X_{\text{concat}}$ 
3: for  $j = 1$  to  $S$  do
4:    $X_{s_j} \leftarrow l_{s_j}.\text{encode}(s).\text{ids}$  (already includes [BOS] and [EOS])
5: end for
6: Build concatenated ids:
7:    $X_{\text{concat}} \leftarrow [\text{bos\_id}]$ 
8: for  $j = 1$  to  $S$  do
9:   Append the inner ids of  $X_{s_j}$  (drop its BOS/EOS):  $X_{s_j}[2:-1]$ 
10:  if  $j < S$  then
11:    Append concat_id
12:  end if
13: end for
14: Append eos_id
15: NTP loss masking: exclude [BOS], [EOS], [CONCAT] positions from prediction targets (implementation typically sets labels to  $-100$  on these ids).
16: Padding/truncation: pad with [PAD] to max length; if truncating, keep the boundary tokens [BOS] and [EOS].

```

B. Theoretical Derivations

Overview. This section corresponds to the theoretical analysis in Sec. 3.3 and the supporting arguments referenced in Secs. 3.1 and 3.2.1. It supplements the main text with derivation-level details of (1) the DPI-based proof for the information loss induced by stochastic corruption (Proposition 3.1; Sec. B.1), (2) the direct supervision density / target-coverage counting under NTP vs. masked modeling in the multi-scale setting (Sec. B.2), and (3) the explicit structural-bias formulation that contrasts graph-transformer static bias with CamS causal constraint plus learned aggregation (Eq. (11); Sec. B.3).

B.1. Proof of Proposition 3.1 (Context Information)

We formalize the conditioning-information gap between (1) uncorrupted evidence and (2) randomly masked evidence.

Setup. For predicting token x_t , let Z_t denote an **unmasked** evidence set (a collection of tokens) and let $\tilde{Z}_t = \mathcal{M}(Z_t)$ be its stochastically masked version under a masking channel \mathcal{M} (e.g., random node/substructure masking used in MLM/MNP). This yields a Markov chain

$$x_t \longleftrightarrow Z_t \longrightarrow \tilde{Z}_t. \quad (14)$$

Proof. By the Data Processing Inequality (DPI), for any Markov chain $X \leftrightarrow Z \rightarrow \tilde{Z}$ we have $I(X; Z) \geq I(X; \tilde{Z})$. Applying DPI with $X = x_t$, $Z = Z_t$, and $\tilde{Z} = \tilde{Z}_t$ gives

$$I(x_t; Z_t) \geq I(x_t; \tilde{Z}_t), \quad (15)$$

which proves Proposition 3.1. \square

Remark (MLM limitations in NLP). XLNet points out two intrinsic issues of corruption-based MLM: (1) the special token corruption (e.g., [MASK]) creates a pretrain–finetune discrepancy, and (2) predicting multiple masked positions with a factorized objective effectively neglects their conditional dependencies given the unmasked context (Yang et al., 2019). Relatedly, ELECTRA shows that much of the compute/sample-efficiency gap of MLM stems from defining the loss only on a small masked subset rather than all positions, while the [MASK] mismatch contributes a smaller but non-negligible part (Clark et al., 2020).

Why this matters more on graphs (evidence-pattern uncertainty). On graphs, the most predictive evidence for a token often lies in its local neighborhood (e.g., bond context, ring connectivity, functional-group surroundings). Random masking can therefore remove not only the target token but also its critical neighborhood evidence, making the **missingness pattern** itself a stochastic nuisance. This motivates a line of graph-pretraining designs that explicitly trade masking density for context stability: (1) masking structured units and adding global knowledge nodes (KPGT) (Li et al., 2023), (2) masking local subgraphs and predicting contextual properties (GROVER) (Rong et al., 2020), and (iii) structure-guided / curriculum masking rather than purely random masking (StructMAE) (Liu et al., 2024). These methods can be interpreted as efforts to find better operating points on the fundamental corruption–prediction trade-off of masked modeling (Wettig et al., 2023).

CamS implication. For CamS, coarse-scale token prediction under NTP conditions on an uncorrupted fine-to-coarse history by construction. Thus, relative to MNP which observes \tilde{Z}_t , CamS provides a higher-SNR conditioning set Z_t that avoids stochastic evidence deletion. This does **not** claim that an arbitrary prefix always dominates the full bidirectional context; rather, it claims that **masking as corruption** strictly reduces the information of whatever evidence set is available, and CamS is designed so that the evidence set for coarse tokens is both uncorrupted and structurally aligned with the fine-grained neighborhood evidence.

B.2. Direct Supervision Density Analysis (Multi-Scale)

As a heuristic proxy for the richness of the learning signal, we compare the density of **direct** token-level supervision signals and how they accumulate over optimization.

Multi-scale notation. Let the multi-scale CamS sequence consist of S scales with lengths $\{T_s\}_{s=1}^S$ and total tokens $T_{\text{all}} = \sum_{s=1}^S T_s$.

Where gradients originate. Let \mathcal{L} be the token-level loss.

- **MNP:** Direct loss terms (hence gradient sources) occur only on masked indices $i \in \mathcal{M}$; unmasked tokens receive gradients only indirectly via attention coupling.
- **NTP:** Direct loss terms occur at (almost) all positions $t \in \{1, \dots, T_{\text{all}} - 1\}$.

Direct supervision density and accumulation. We define the **Direct Supervision Density** (SD) as the expected fraction of tokens that serve as prediction targets per update:

$$SD_{\text{NTP}} \approx 1, \quad SD_{\text{MNP}} = \rho. \quad (16)$$

Equivalently, over K optimization steps, the number of direct token-level targets scales as

$$\mathcal{R}_{\text{NTP}} \propto K \cdot T_{\text{all}}, \quad \mathcal{R}_{\text{MNP}} \propto K \cdot \rho T_{\text{all}}. \quad (17)$$

Thus, NTP provides about $1/\rho$ times more direct targets than MNP (e.g., $6.7\times$ when $\rho = 0.15$).

Trade-off and practical masking rates. Increasing ρ increases the number of predictions but also increases corruption, forming a fundamental trade-off in masked modeling (Wettig et al., 2023). In molecular graph Transformers, KPGT reports that setting the masking rate to $\rho = 0.5$ can be optimal when token design and global knowledge tokens help stabilize the conditioning context (Li et al., 2023). More broadly, structured masking / task design in graph pretraining (e.g., GROVER) can be viewed as attempts to obtain more useful target coverage without excessively destabilizing the evidence set (Rong et al., 2020).

Why dense (and repeated) supervision can help. Dense token-level objectives are known to improve sample efficiency compared to losses defined only on a small masked subset; ELECTRA explicitly attributes a major part of MLM’s inefficiency to learning from only masked tokens rather than all positions (Clark et al., 2020). CamS strengthens this further via **multi-view repetition**: the same molecule contributes token-level targets repeatedly across scales, inducing cross-scale consistency pressure and providing redundant evidence pathways (a motif may appear as fine tokens at small scales and as a merged token at larger scales). This reduces sensitivity to any single tokenization granularity and makes the effective supervision more robust.

B.3. Structural Bias Formulation

We distinguish the structural injection mechanism in Eq. (11).

Graphformer (Hard Static Bias). The bias ψ_{ij} is defined via static structural encodings (e.g., shortest-path distance), injected into attention as an additive bias term (Ying et al., 2021):

$$\psi_{ij}^{\text{Graph}} = b_{\phi(d_G(i,j))}. \quad (18)$$

CamS (Hard Causal Constraint + Soft Learned Aggregation). CamS uses a hard causal mask to enforce fine-to-coarse information flow:

$$\psi_{ij}^{\text{CamS}} = \begin{cases} 0 & \text{if } (i \rightarrow j) \text{ is allowed by } \mathbf{M}_{\text{causal}} \\ -\infty & \text{otherwise.} \end{cases} \quad (19)$$

Within the permitted region, connectivity is **content-adaptive** via $\mathbf{q}_i^\top \mathbf{k}_j$; hence coarse-scale tokens learn which fine-scale neighborhood details to aggregate, rather than uniformly mixing neighbors at a given distance.

C. Training and Implementation Details

Overview. This section corresponds to the training and evaluation protocols in Secs. 3.2.1 and 4. It supplements the main text with implementation-level details of (1) the shared training framework and parallelization setup for pre-training vs. fine-tuning (Sec. C.1), (2) the complete pre-training configuration on Enamine675M (MultiScaler3375M) (Table 5), (3) the fixed fine-tuning setup used across MoleculeNet and MoleculeACE (Table 6), and (4) the unified hyperparameter search space (including strategy-specific grids) (Table 7).

C.1. Pre-training and Fine-tuning Hyperparameters

Implementation and framework. All experiments are implemented in PyTorch using HuggingFace Transformers. Pre-training uses the built-in `Trainer` with DeepSpeed ZeRO-2 on multi-GPU data parallelism; fine-tuning is run as single-GPU jobs (one job per GPU) using the same `Trainer` API (or strategy-specific subclasses).

Pre-training on Enamine675M (MultiScaler3375M). We pre-train a 16-layer LLaMA-style decoder initialized **from a local config** (i.e., random initialization; no pretrained weights are loaded). The training data are pre-tokenized and stored as HuggingFace datasets on disk with train/validation splits. We use FP16 training with a cosine learning-rate schedule and warmup, and evaluate/save checkpoints periodically during training.

Fine-tuning (MoleculeNet and MoleculeACE). We fine-tune the pretrained backbone with fingerprint injection (`fp_dim=2048`) and a lightweight supervised head. All downstream runs use FP16, evaluate every epoch, and select the best checkpoint by the primary validation metric (higher-is-better for AUROC; lower-is-better for RMSE). We also tested two dropout application schemes in the MoleculeACE fine-tuning pipeline: (1) **head-only** dropout (applied only in the supervised head), and (2) **backbone-synced** dropout (also overriding backbone `attention_dropout/hidden_dropout` and all `nn.Dropout` modules). Both schemes share the same dropout-rate grid in Table 7.

Ablation compute budget. For ablations (e.g., single-scale tokenization or removing fingerprint injection), we keep the optimizer, LR schedule, batch size, and training length the same as the corresponding main setting, and only change the ablated component.

Table 5. Pre-training hyperparameters on Enamine675M (MultiScaler3375M).

Setting	Value
Backbone config	16 layers; hidden size 720; 8 heads; MLP 2880
Context length	4096 (<code>max_position_embeddings</code>)
Initialization	new model from local config (no pretrained weights)
Tokenizer	CamS-tokenizer; embedding resized to <code>tokenizer.vocab_size</code>
Training instances	Multi-scale tokenized corpus (MultiScaler3375M; 5 views per molecule)
Parallelism	<code>torchrun 8 processes + DeepSpeed ZeRO stage 2</code>
Precision	FP16 (<code>fp16=true</code> in Trainer and DeepSpeed)
Micro-batch size	256 per GPU
Gradient accumulation	2
Global batch size	4096 ($256 \times 8 \times 2$)
Optimizer	AdamW (Transformers Trainer default)
Learning rate	1×10^{-4}
Weight decay	1×10^{-2}
LR schedule	cosine; <code>warmup_steps = 5000</code>
Gradient clipping	1.0 (DeepSpeed <code>gradient_clipping</code>)
Training length	10 epochs in planning (early stop after 1/10 epoch in actual execution)
Eval / save / log	<code>eval_steps = 33000; save_steps = 33000; logging_steps = 3300</code>
Checkpoint cap	<code>save_total_limit = 100</code>

Table 6. Fixed fine-tuning setup for MoleculeNet and MoleculeACE.

Setting	MoleculeNet	MoleculeACE
Task type	classification / regression (per dataset)	regression
Data split	provided scaffold splits (same as KPGT), fold $\in \{0, 1, 2\}$	provided scaffold splits (same as KPGT)
Epochs	80 (search phase)	50
Batch size	32 per GPU (default)	32 per GPU (default; a small subset rerun with 64)
Grad accumulation	1 (default)	1 (default)
Optimizer	AdamW (Trainer default)	AdamW (Trainer default)
LR schedule	constant_with_warmup, warmup_ratio = 0.1	constant_with_warmup, warmup_ratio = 0.1
Evaluation	per epoch	per epoch
Primary metric	AUROC / macro-AUROC; RMSE for regression tasks	RMSE (overall_RMSE)

Table 7. Fine-tuning hyperparameter search space (shared).

Hyperparameter	Candidates
Base grid (48 combos)	learning_rate $\in \{10^{-6}, 3 \times 10^{-6}, 10^{-5}, 3 \times 10^{-5}\}$ dropout_rate $\in \{0, 0.05, 0.1, 0.2\}$; weight_decay $\in \{0, 10^{-6}, 10^{-4}\}$
Fine-tune strategy	normal, l2sp, llrd, flag, reinit
LLRD	layer_decay $\in \{0.95, 0.9, 0.85, 0.8\}$
L2SP	weight $\in \{10^{-1}, 10^{-2}, 10^{-3}, 10^{-4}\}$
FLAG	$\epsilon \in \{10^{-3}, 3 \times 10^{-3}, 5 \times 10^{-3}, 10^{-2}\}$
Reinit	reinit_num_layers $\in \{1, 2, 3, 4\}$

D. Detailed Experimental Results

Overview. This section corresponds to the benchmark results summarized in Sec. 4. It supplements the main text with the full detailed tables of (1) MoleculeNet overall performance of all baseline and their rank comparison (extended version of Table 1; Table 8), and (2) MoleculeACE results overall performance of all baseline and their rank comparison (extended version of Table 2; Table 9).

Table 8. Full Performance comparison on MoleculeNet benchmark. (Extended version of Table 1). Sup variants: $_{sup}$ denotes adding an additional supervised graph-level bioactivity pre-training stage on top of the corresponding self-supervised objective (same protocol as used in the baseline setting). Baseline Reference: Infomax (Veličković et al., 2018); Edgepred (Hamilton et al., 2017); Attribute Masking (Masking) (Hu et al., 2020); Context Prediction (Contextpred) (Hu et al., 2020); GraphLoG (Xu et al., 2021); GraphCL (You et al., 2020); JOAO (You et al., 2021); GROVER (Rong et al., 2020); 3DInfomax (Stärk et al., 2022); GraphMVP (Liu et al., 2016); ImageMol (Zeng et al., 2022); MolFormer (Wu et al., 2023); GEM (Fang et al., 2022); GraphMAE (Hou et al., 2022); MoleBert (Xia et al., 2023); KPGT (Li et al., 2023)

Classification Tasks			Regression Tasks		
Method	AVG-AUROC \uparrow	Rank	Method	AVG-RMSE \downarrow	Rank
CamS-LLaMA	0.845	1	CamS-LLaMA	1.172	1
KPGT	0.843	2	KPGT	1.175	2
CamS-LLaMA (w/o FP)	0.838	3	CamS-LLaMA (w/o FP)	1.195	3
CamS-LLaMA (Vocab-1K Only)	0.833	4	CamS-LLaMA (Vocab-1K Only)	1.215	4
GEM	0.825	5	MolFormer	1.272	5
CamS-LLaMA (Vocab-67K Only)	0.818	6	GEM	1.285	6
GROVER	0.818	7	CamS-LLaMA (Vocab-67K Only)	1.329	7
Contextpred $_{sup}$	0.807	8	GROVER	1.332	8
3DInfomax	0.804	9	3DInfomax	1.400	9
ImageMol	0.802	10	Contextpred $_{sup}$	1.414	10
MoleBERT	0.802	11	ImageMol	1.501	11
Masking $_{sup}$	0.799	12	MoleBERT	1.559	12
Edgepred $_{sup}$	0.795	13	Contextpred	1.563	13
Infomax $_{sup}$	0.794	14	Edgepred $_{sup}$	1.576	14
JOAO	0.790	15	Masking $_{sup}$	1.620	15
Contextpred	0.790	16	GraphMVP	1.647	16
GraphMAE	0.788	17	Infomax $_{sup}$	1.661	17
Edgepred	0.785	18	GraphLoG	1.663	18
GraphCL	0.774	19	Edgepred	1.674	19
Infomax	0.773	20	Masking	1.697	20
Masking	0.773	21	GraphMAE	1.716	21
GraphLoG	0.769	22	Infomax	1.770	22
GraphMVP	0.769	23	GraphCL	1.822	23
MolFormer	0.744	24	JOAO	1.960	24

Table 9. Full Detailed results on 30 MoleculeACE activity-cliff tasks (Regression, RMSE \downarrow). (Extended version of Table 2). Sup variants: $_{sup}$ denotes adding an additional supervised graph-level bioactivity pre-training stage on top of the corresponding self-supervised objective (same protocol as used in the baseline setting). Descriptors: ECFP (Rogers & Hahn, 2010); MACCS (Durant et al., 2002); PHYSCHEM (Walters & Murcko, 2002); WHIM (Kubinyi, 1993). Baseline Reference: support vector machines (SVM) (Cristianini & Scholkopf, 2002); random forest (RF) (Breiman, 1996); gradient boosting machine (GBM) (Friedman, 2001); k-nearest neighbor (KNN) (Fix, 1985); message passing neural network (MPNN) (Gilmer et al., 2017); graph attention network (GAT) (Veličković et al., 2017); graph convolutional network (GCN) (Kipf, 2016); AFP (Xiong et al., 2019); Convolutional Neural Network Long Short-Term Memory (CNN, specifically Maxsmi) (Kimber et al., 2021); Long Short-Term Memory (LSTM, specifically CLM) (Moret et al., 2022); Transformer (specifically Chemberta) (Chithrananda et al., 2020); KPGT (Li et al., 2023)

MoleculeACE AVG-RMSE (Ranks 1–24)			MoleculeACE AVG-RMSE (Ranks 25–48)		
Method	AVG-RMSE \downarrow	Rank	Method	AVG-RMSE \downarrow	Rank
CamS-LLaMA	0.624	1	EdgePred $_{Sup}$	0.764	25
KPGT	0.633	2	Contextpred $_{Sup}$	0.764	26
CamS-LLaMA (Vocab-1K Only)	0.641	3	GraphMVP	0.768	27
CamS-LLaMA (Vocab-67K Only)	0.649	4	Infomax	0.774	28
CamS-LLaMA (w/o FP)	0.650	5	Edgepred	0.774	29
SVM $_{ECFP}$	0.675	6	ImageMol	0.797	30
GROVER	0.680	7	3DInfomax	0.804	31
GBM $_{ECFP}$	0.701	8	GraphLoG	0.807	32
RF $_{ECFP}$	0.705	9	KNN $_{MACCS}$	0.818	33
MolFormer	0.740	10	GEM	0.821	34
KNN $_{ECFP}$	0.741	11	Transformer	0.868	35
MLP $_{ECFP}$	0.742	12	RF $_{PHYSCHEM}$	0.890	36
GBM $_{MACCS}$	0.742	13	GBM $_{PHYSCHEM}$	0.901	37
LSTM	0.744	14	KNN $_{PHYSCHEM}$	0.923	38
Contextpred	0.747	15	SVM $_{PHYSCHEM}$	0.935	39
RF $_{MACCS}$	0.753	16	CNN	0.937	40
GraphMAE	0.753	17	MPNN	0.959	41
SVM $_{MACCS}$	0.754	18	AFP	0.970	42
Masking $_{Sup}$	0.755	19	RF $_{WHIM}$	0.977	43
MoleBERT	0.755	20	GBM $_{WHIM}$	0.992	44
Infomax $_{Sup}$	0.756	21	SVM $_{WHIM}$	1.003	45
JOAO	0.757	22	GCN	1.010	46
Masking	0.758	23	KNN $_{WHIM}$	1.020	47
GraphCL	0.760	24	GAT	1.049	48

E. Interpretability Details for Activity-Cliff Attention Analysis

Overview. This section corresponds to the activity-cliff attention analysis in Sec. 4.3. It supplements the main text with implementation-level details of (1) activity-cliff pair construction and differential/shared atom identification (Appendix E.1), Alg.7, (2) mapping atom-level diff/shared labels to CamS tokens within each scale region (Appendix E.2), and (3) attention extraction and metric computation/aggregation for MDTA/MSTA and Rel-DTAP (Appendix E.3).

E.1. Activity-cliff Pair Construction and Differential/Shared Atom Identification

Pair construction (MoleculeACE-style). For each MoleculeACE sub-task dataset, we start from its per-molecule CSV containing `smiles`, `exp_mean [nM]`, `cliff_mol`, and the split label. We treat molecules with `cliff_mol=1` as anchors (by default restricted to the test split), and search partners among molecules with `cliff_mol=0` (by default from the same split). A candidate pair is kept if it satisfies both (1) **high structural similarity** and (2) **large potency change**. Structural similarity is a “soft-consensus” rule: we compute (a) full-molecule ECFP Tanimoto, (b) generic Murcko-scaffold ECFP Tanimoto, and (c) SMILES Levenshtein similarity, and accept the pair if **any** of them is $\geq \tau_{\text{sim}}$ (default 0.9). Potency change is measured by the fold change on linear `exp_mean [nM]` values: $\text{FC} = \frac{\max(y_a, y_p)}{\max(\min(y_a, y_p), \epsilon)}$ (with $\epsilon=10^{-12}$), and we keep the pair if $\text{FC} \geq \tau_{\text{fold}}$ (default 10). Each selected pair yields one record (anchor, partner); for downstream attention statistics we count the two molecules (anchor and partner) separately, as stated in Sec. 4.3.

Differential vs. shared atoms. Given an (anchor, partner) pair, we identify shared atoms via an RDKit maximum common substructure (MCS) query with ring constraints and chemistry-aware matching (elements compared by type; bonds compared by order; `completeRingsOnly` and `ringMatchesRingOnly` enabled). Let \mathcal{A} and \mathcal{B} be the atom-index sets of the two molecules and let $\mathcal{M} \subseteq \mathcal{A}$ and $\mathcal{M}' \subseteq \mathcal{B}$ be the matched atom indices returned by the first substructure match of the MCS query. We define **differential atoms** as the complement sets $\mathcal{A}_\Delta = \mathcal{A} \setminus \mathcal{M}$ and $\mathcal{B}_\Delta = \mathcal{B} \setminus \mathcal{M}'$, and **shared atoms** as \mathcal{M} and \mathcal{M}' . If MCS fails (or a SMILES cannot be parsed), we conservatively treat all atoms as differential.

Atom correspondence (optional for visualization). For visualization/debugging we also record the ordered atom correspondence induced by the MCS query, i.e., a list of paired indices $\{(i, j)\}$ obtained by aligning the two match tuples in the MCS SMARTS query order. This mapping is not required for computing Rel-DTAP, but enables atom-level highlighting across the two molecules.

E.2. Mapping Atom-level Diff/Shared Labels to Tokens in Each Scale Region

Token-to-atom alignment. We re-encode each molecule with `MultiGraphBPETokenizerExplain`, which returns, for every token position t , an atom-index set S_t indicating which RDKit atom indices are covered by that token (special tokens such as `[BOS]`, `[EOS]`, and `[CONCAT]` have empty sets). Because GraphBPE encoding inserts auxiliary connector atoms (`*`) with indices outside the original RDKit atom range, we remove such indices by clipping S_t to $\{0, \dots, N-1\}$ where N is the number of atoms in the original molecule.

From atom-level labels to token-level labels. Let \mathcal{A}_Δ be the differential-atom set for this molecule from Appendix E.1. We assign a token-level differential indicator by an **any-diff** rule: a token at position t is marked as differential iff $S_t \cap \mathcal{A}_\Delta \neq \emptyset$; otherwise it is marked as shared/non-differential. Thus a token covering multiple atoms is counted as differential if it contains at least one differential atom.

Scale-region boundaries in the concatenated sequence. For multi-scale CamS sequences, scale regions are delimited by the `[CONCAT]` separators. Concretely, given the full token-id list (including `[BOS]`, `[EOS]`, and `[CONCAT]`), we split it into consecutive spans between `[CONCAT]` tokens, and exclude `[BOS]`/`[EOS]`/`[CONCAT]` themselves from the per-region statistics. This yields the four scale regions (e.g., 1K/7K/27K/67K in the paper) used to report scale-wise attention preferences.

E.3. Attention Extraction and Metric Computation

Attention extraction protocol. For each molecule, we run a forward pass with `output attentions=True` and extract the **last-layer** attention tensor. We average over heads to obtain a single attention matrix $\bar{\mathbf{A}} \in \mathbb{R}^{S \times S}$, where S is the sequence length. We use the attention distribution of the final token (the last position in the sequence) as a saliency-like

weighting over the prefix tokens, i.e., the row vector $\bar{\mathbf{A}}_{S,:}$. We compute this distribution in two modes: (1) **without fingerprint input** by running the model without the prepended fingerprint token; (2) **with fingerprint input** by prepending the fingerprint embedding (sequence length becomes $S+1$), extracting $\bar{\mathbf{A}}_{S+1,:}$, and then taking only the sub-vector over molecular tokens (excluding the fingerprint position) for diff/shared statistics.

MDTA/MSTA within a scale region. Within a given scale region s (defined by [CONCAT] boundaries), let p_i denote the (renormalized) attention weight on token i in that region, and let $d_i \in \{0, 1\}$ be its differential indicator from Appendix E.2. We define the mean differential-token attention and mean shared-token attention as

$$\text{MDTA}_s = \frac{\sum_i p_i d_i}{\sum_i d_i}, \quad \text{MSTA}_s = \frac{\sum_i p_i (1 - d_i)}{\sum_i (1 - d_i)},$$

with the convention that the corresponding mean is set to 0 if the denominator is 0 (no tokens of that type in the region).

Rel-DTAP computation and aggregation. For each molecule (anchor and partner counted separately), we compute

$$\text{Rel-DTAP}_s = \frac{\text{MDTA}_s - \text{MSTA}_s}{\text{MSTA}_s + \epsilon} \times 100,$$

using $\epsilon = 10^{-12}$ for numerical stability. We report the final Rel-DTAP by averaging this quantity over all molecules from activity-cliff pairs, both for each scale region s and for the full concatenated sequence (all regions combined).

Algorithm 7 Shared/differential fragment labeling for an activity-cliff pair

- 1: **Input:** SMILES pair (s_a, s_b) ; RDKit MCS; tokenizer-explain encoder ι returning per-token atom sets
- 2: **Output:** shared/diff atom sets (M_a, Δ_a) and (M_b, Δ_b) ; token-level diff masks $\mathbf{d}^{(a)}, \mathbf{d}^{(b)}$; optional atom map \mathcal{P}
- 3: $m_a \leftarrow \text{MolFromSmiles}(s_a)$; $m_b \leftarrow \text{MolFromSmiles}(s_b)$
- 4: $N_a \leftarrow m_a.\text{GetNumAtoms}()$; $N_b \leftarrow m_b.\text{GetNumAtoms}()$
- 5: $\text{smarts} \leftarrow \text{FindMCS}([m_a, m_b];$
 completeRingsOnly, ringMatchesRingOnly,
 CompareElements, CompareOrder).smartsString
- 6: **if** smarts is empty **then**
- 7: $M_a \leftarrow \emptyset$; $M_b \leftarrow \emptyset$
- 8: **else**
- 9: $q \leftarrow \text{MolFromSmarts}(\text{smarts})$
- 10: $\mathbf{t}_a \leftarrow m_a.\text{GetSubstructMatch}(q)$; $\mathbf{t}_b \leftarrow m_b.\text{GetSubstructMatch}(q)$ (take the first match)
- 11: $M_a \leftarrow \text{set}(\mathbf{t}_a)$; $M_b \leftarrow \text{set}(\mathbf{t}_b)$
- 12: $\mathcal{P} \leftarrow \{(\mathbf{t}_a[i], \mathbf{t}_b[i])\}_{i=1}^{|\mathbf{t}_a|}$ (ordered atom correspondence)
- 13: **end if**
- 14: $\Delta_a \leftarrow \{0, \dots, N_a - 1\} \setminus M_a$; $\Delta_b \leftarrow \{0, \dots, N_b - 1\} \setminus M_b$
- 15: **for** side $m \in \{a, b\}$ **do**
- 16: Encode s_m with ι to get tokens $(x_1^{(m)}, \dots, x_{L_m}^{(m)})$ and atom sets $\{S_t^{(m)}\}_{t=1}^{L_m}$
- 17: Clip connector atoms: $S_t^{(m)} \leftarrow S_t^{(m)} \cap \{0, \dots, N_m - 1\}$ for all t
- 18: **for** $t = 1$ **to** L_m **do**
- 19: **if** $x_t^{(m)}$ is [BOS] or [EOS] or [CONCAT] **then**
- 20: $d_t^{(m)} \leftarrow 0$
- 21: **else**
- 22: **if** $S_t^{(m)} \cap \Delta_m \neq \emptyset$ **then**
- 23: $d_t^{(m)} \leftarrow 1$ (diff fragment token; any-diff rule)
- 24: **else**
- 25: $d_t^{(m)} \leftarrow 0$ (shared fragment token)
- 26: **end if**
- 27: **end if**
- 28: **end for**
- 29: **end for**
